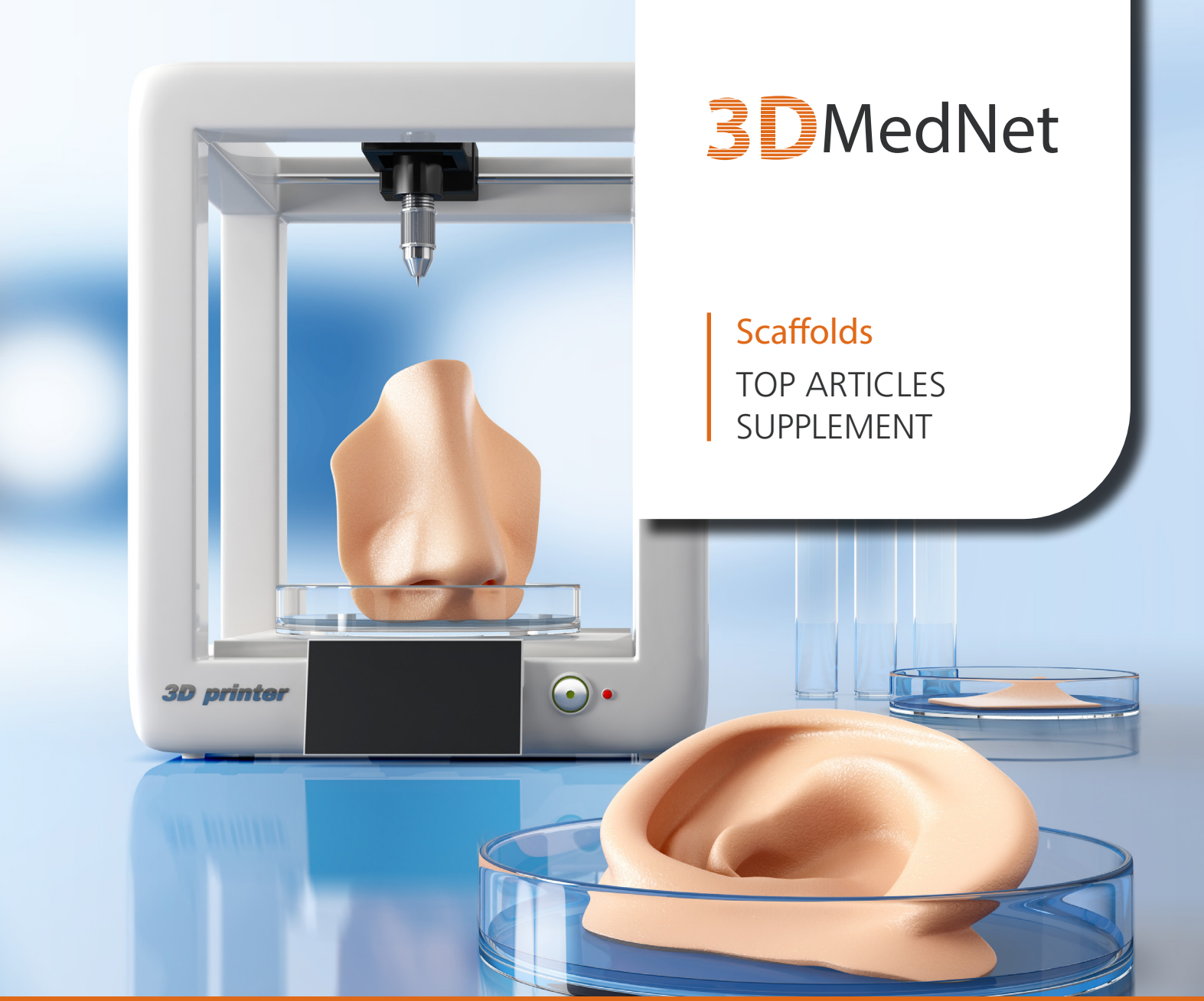

3DMedNet

Scaffolds

TOP ARTICLES SUPPLEMENT

CONTENTS

fsg CONNECT

Short Communication

For reprint orders, please contact: reprints@futuremedicine.com

Journal of
3D Printing in Medicine

In situ functionalization of scaffolds during extrusion-based 3D plotting using a piezoelectric nanoliter pipette

Stefan Giron[1], Anja Lode[1] & Michael Gelinsky*[,1]

[1]Centre for Translational Bone, Joint & Soft Tissue Research, University Hospital Carl Gustav Carus & Faculty of Medicine, Technische Universität Dresden, Fetscherstr. 74, 01307 Dresden, Germany

*Author for correspondence: michael.gelinsky@tu-dresden.de

Additive manufacturing techniques can be applied to individually craft medical implants and biomaterial scaffolds. We present the combination of macroscopic scaffold fabrication by strand deposition and high-resolution dosing of liquids using the 'BioScaffolder 2.1' 3D plotter from GeSiM with an integrated piezoelectric nanoliter pipette. A fluorescein solution, used as model substance, was dispensed on calcium phosphate bone cement strands during scaffold production; high reproducibility of the alternating subprocesses was demonstrated. Moreover, the release kinetics of VEGF loaded onto flat calcium phosphate cement substrates was investigated. The presented approach opens up new and exciting possibilities for tissue engineering. Various biological components can be integrated precisely into 3D scaffolds according to a predefined pattern creating tissue equivalents of high complexity.

First draft submitted: 7 June 2016; Accepted for publication: 30 August 2016; Published online: 13 October 2016

Keywords: 3D printers • drug delivery • technology

In recent years, additive manufacturing techniques have become a promising approach in regenerative medicine. Especially, 3D printing with modified inkjet printers has allowed creating well-designed living constructs thanks to the high-resolution positioning of small droplets of bioink and ease of use [1]. However, this method is restricted by the low viscosity of suitable bioinks, resulting in rather flat geometries [1,2]. In contrast, extrusion-based 3D printing or 3D plotting offers the opportunity to process a broad range of different pasty materials with high viscosities under mild conditions [3–5]. Therefore, fabrication of scaffolds with dimensions of several centimeters is possible. The mild process conditions basically allow the integration of biological factors. However, this might require complex additional steps for loading [6,7] and drastically reduces the number of suitable materials – the latter, especially if cells should be incorporated. In this work, the 3D plotting technique was expanded by adding a piezoelectric dispensing device with the aim to functionalize the 3D scaffolds during their manufacturing.

Although the plotting process results in macroscopic constructs, they may be easily modified with solutions of various different substances on a submillimeter scale. Thus, local patterning with drugs or active substances like growth factors to guide cell adhesion or cell fate using printing technologies previously mostly limited to 2D substrates now becomes possible during fabrication of 3D scaffolds. Besides this alternative loading method without the need to mix the biological component into the plotting paste and thereby defining its concentration, this approach also facilitates the localized deposition of different cell types.

In this study, we have chosen a pasty, self-setting calcium phosphate bone cement (CPC) as plotting material and an aqueous fluorescein solution as model substance for local modification during scaffold

Future Medicine part of fsg

fabrication. Additionally, a release experiment with VEGF was conducted to test whether the method of application possibly interferes with the agent in use. Recently, we have shown homogeneous functionalization of the same type of CPC with VEGF by mixing of both components prior to manufacturing of 3D scaffolds for bone tissue engineering by 3D plotting [7].

Materials & methods

Scaffold fabrication by 3D plotting

3D plotting was carried out using a commercially available BioScaffolder 2.1 from GeSiM (Radeberg, Germany) with an integrated 'Nano Tip' piezoelectric pipetting unit. An α-tricalcium phosphate-based hydroxyapatite forming CPC (Velox™ from InnoTERE, Radebeul, Germany) was used as plotting paste in which the solid precursor mixture is suspended in an oily liquid [4,8]. The paste was extruded from a cartridge (NordsonEFD, Dunstable, UK) via a dosing needle with an inner diameter of 610 µm (Globaco, Roedermark, Germany) using compressed air at a pressure of 250 kPa and a speed of 9.7 mm/s. The strands were deposited layer by layer according to a predefined layout realizing the 3D scaffold. To cut off the strands at the end, a horizontal tear off of 3 mm was implemented with a tear-off speed of 30 mm/s.

Integration of piezoelectric pipetting into the 3D plotting process

A 0.1 mM fluorescein solution that had been prepared from fluorescein diacetate (Sigma-Aldrich, Taufkirchen, Germany) according to McKinney *et al.* [9] was used as a model liquid to test the ability to combine 3D plotting and pipetting. The solution was picked up from a 96-well tissue culture polystyrene (TCPS) plate (Greiner Bio-One, Frickenhausen, Germany) directly before pipetting using the piezoelectric pipetting unit with a so-called 'Nano Tip' (GeSiM). An integrated stroboscope was used to check the dispensing behavior. Theoretically, the size of dispensed drops may be adjusted by changing the pulse length and voltage applied to the pipette's piezo actor. In practice, these parameters were used to adjust the fluid properties of the dispensed liquids and minor differences of the pipette in use in order to guarantee reproducible dispensing of drops consisting of about 0.5 nl each. The applied voltage was 70 V at a frequency of 100 Hz and a width of 60 µs for the rectangular pulse. To increase the dispensed volume, several drops were put on the same position.

The movement of both the devices, the plotting cartridge and the piezopipette, was controlled by the three-axis motion system of the BioScaffolder. The actual pipetting was carried out when the pipette was at rest. First, a layer of three parallel CPC strands was plotted. Second, fluorescein solution was pipetted on top of these strands. Third, a second layer of CPC was put onto the strands of the first layer creating perpendicular crossings. Fourth, fluorescein was pipetted on the strands of the second layer and so forth until eight layers of CPC were deposited in total. The intended layout is sketched in Figure 1A.

Light microscopy

Images were recorded with a Leica M205C stereomicroscope (Leica Microsystems, Wetzlar, Germany). The GNU Image Manipulation Program (GIMP, version 2.8.10) [10] was used for image processing.

Release experiment

In order to check whether the pipetting alters the release kinetics, recombinant human VEGF-A_{165} (Biomol, Hamburg, Germany) was pipetted on preset CPC samples. A concentration of 100 µg/ml was used with the 'Nano Tip' and 10 µg/ml with conventional pipettes ('Research,' Eppendorf, Hamburg, Germany). The samples were prepared from the same CPC paste used for 3D plotting. Those flat disks with 10-mm diameter and 1-mm height were produced with a silicone mold and had been set in water-saturated atmosphere at 37°C for 3 days [7]. Afterward, the CPC disks have been washed twice, disinfected by immersion in 70% ethanol for 15 min and rinsed again with 70% ethanol before air drying. All samples were placed in 48-well TCPS plates (Nalge Nunc International, Roskilde, Denmark), which had been incubated with 1% bovine serum albumin (Sigma-Aldrich) in phosphate-buffered saline (Gibco Life Technologies, CA, USA) overnight in order to prevent binding of VEGF to the plastic surface. The VEGF solution was prepared in a 96-well TCPS plate (Greiner) that was also incubated overnight with 1% bovine serum albumin in phosphate-buffered saline. Four samples were loaded with 46-ng VEGF each by dispensing a simple pattern of 1000 drops of about 0.46 nl with the piezoelectric pipette. Three controls with 50 ng have been prepared using manual pipetting and one CPC disk without VEGF was used as negative control. The release was started 30 min after the pipetting using α-minimum essential medium (MEM; BioChrom, Berlin, Germany) with 9% fetal calf serum as the release medium. After 2 h and afterward every 24 h, the release medium has been replaced for a total release interval of 7 days. The amount of released VEGF was determined by an ELISA following standard protocols described previously [11].

Although the release experiment was carried out under cell-culture conditions, the pipetting itself was not strictly sterile in the current setup of the

BioScaffolder. Though operated in a sterile workbench, the pipetting unit could only be disinfected by rinsing the pipette and the tubes of the hydraulic system with 70% ethanol for several minutes. Automatic cleaning procedures used the so-called 'system water' that was in contact with the pipette and the tubes, breaking sterility. Nonetheless, no contamination has occurred, neither in the release experiment, nor in experiments with living cells not described here.

Results & discussion

It could be demonstrated in previous studies [4,7] that the CPC, used here as biomaterial for scaffold fabrication, is a suitable pasty material for extrusion-based 3D plotting. As it is a self-setting material, no other treatment than immersion in aqueous media or contact with humidity is required to form mechanically stable constructs. By varying needle diameter and strand distance as well as strand orientation in neighboring layers, a variety of geometries can easily be realized [4,7,12].

We now have been able to dispense very small volumes of a liquid onto plotted scaffolds *in situ* during the computer-aided manufacturing process under mild conditions. The scaffolds consisting of eight CPC layers, shown in Figure 1, have been realized by alternating 3D plotting and piezopipetting. The plotted strands have been used as the spatial reference for the pipetting process. After calibration, the fluorescein solution could be placed on top of the strands with high accuracy. By varying the number of drops dispensed at each position from 1 to 32, a fluorescein gradient was created. The application of different liquids even in one layer is also feasible; however, it is not shown. As a washing step is necessary when changing the liquid, the remaining volume is wasted and the overall production time is increased. Thus, the number of liquid changes should be minimized by design. Smaller volumes per droplet could be achieved using a 'Pico Tip,' also available as a tool for the GeSiM BioScaffolders.

The presented combination of 3D plotting and pipetting enables us to create scaffolds with complex patterns of functional substances. Though the resolution of the pipetting was shown to be generally excellent, the liquid/material combination always has to be taken into account, especially when fast diffusion of the liquid on or into the underlying strand might occur. The use of hydrogels in former studies [5,13,14] already showed that cells may be directly incorporated into scaffolds with clinically relevant dimensions. With integrated pipetting, the range of scaffold materials that may be seeded with live cells during 3D fabrication can be widened as the cells are not to be immersed in the plotting pastes. Immiscible fluids may also be locally dispensed, as shown with

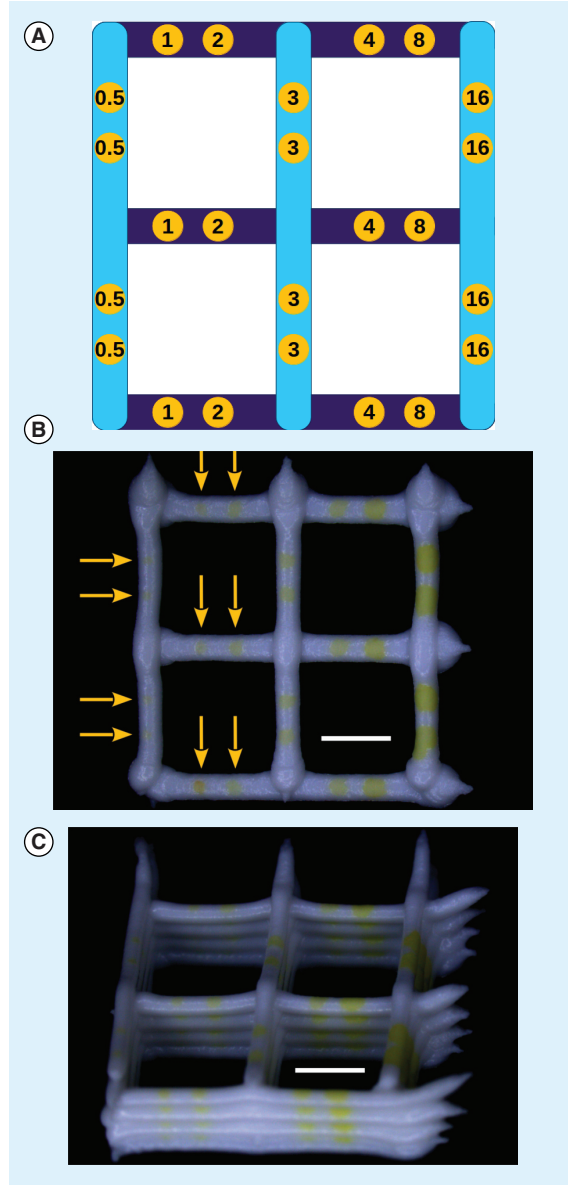

Figure 1. Functionalization of a plotted 3D scaffold during manufacturing with small volumes of a liquid solution. (A) Scheme of the scaffolds shown in parts **(B)** and **(C)** indicating the pipetted volume at each position in nanoliters. The two different colors of the strands represent the two layers, printed on top of each other. **(B)** Light microscopic image of a plotted CPC scaffold with approximately 0.7 mm strand diameter and pipetted spots with 0.1 mM fluorescein solution, visible by its bright yellow color. Arrows point at small spots. The lateral resolution depends highly on the dispensed volume. **(C)** Light microscopic image of a 3D scaffold with eight layers realizing the scheme **(A)** four-times. Note that the fluorescein spots are partially covered by the strands of the following layer. Depending on the pasty material and the chosen geometry, this is not necessarily the case. The resolution in the direction perpendicular to the layers is additionally limited by the strand height. Scale bars correspond to 2 mm. CPC: Calcium phosphate cement.

the water-based fluorescein solution on the oil containing hydrophobic CPC strands. Furthermore, the pipetting allows tailoring of the local concentrations of drugs or biological factors (or the cell seeding density) unlike the homogeneous distribution provided by mixing the plotting paste with the substance or cells, respectively. The pasty materials utilized for 3D plotting are restricted to those that may be processed without buoyancy compensation, in other words, extrusion into a liquid plotting medium [15]. In contrast to inkjet printing and 3D plotting, where the number of different liquids and their combinations is limited by the number of available cartridges, the pipetting enables the local integration of many different substances or even different cell types into one single scaffold. This is possible since the liquids are picked up from 96-well plates during scaffold synthesis. The applicability of the piezoelectric nanoliter pipette for cell positioning was already proven. Jonczyk *et al.* have shown very recently localized cell seeding of the human lung carcinoma cell line A-549 used as model in 2D with a 'NanoPlotter' (GeSiM), utilizing the same pipetting unit [16]. Moreover, we were also able to locally seed cells of an osteosarcoma cell line (SAOS-2) into TCPS well plates as well as on collagen membranes with the BioScaffolder (data not shown).

The VEGF solution, automatically pipetted onto a flat CPC substrate, showed the same release kinetics as the manually pipetted growth factor. The data from ELISA are displayed in Figure 2. In both cases, a large initial burst was observed, releasing approximately 93% of the VEGF within the first 2 h. After 24 h, the release was basically complete. In contrast, a slow and only partial release was observed when VEGF (adhered to chitosan microparticles) was mixed homogeneously with the CPC paste prior to scaffold fabrication by 3D plotting. In this study, preservation of biological activity of the released growth factor was verified in direct and indirect cell culture experiments [7]; therefore, it is very likely that VEGF dosing by piezopipetting does not alter bioactivity as it is a much less invasive process compared with direct inclusion in the plotting paste.

The very quick VEGF release in the present study was due to the short time period of 30 min from loading to release. Lode *et al.* showed in a similar setup that the release would be delayed by longer loading periods [17]. Also a modification by adding heparin to the CPC was shown to result in a slower release with reduced initial burst [17]. Furthermore, the release kinetics might be altered independently from the specific biological factor by enclosing it between strands, either on crossings or in full length, when multiple strands are plotted onto another in the same orientation. Owing to the fact that the liquids can only be dispensed onto the top of the strands, the high resolution of scaffold functionalization can only be achieved on the level of each single layer; perpendicular to the layers, the resolution is limited by the strand diameter. In practice, the resolution depends highly on the dispensed volume and the wetting of the liquid/paste material combination.

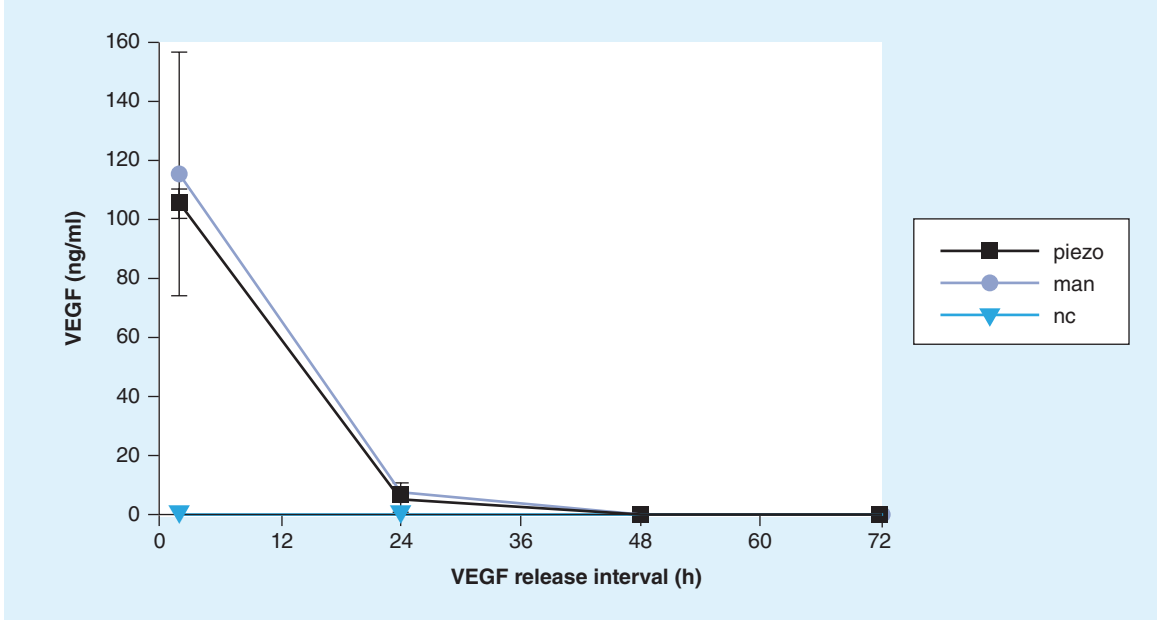

Figure 2. The release kinetics of the samples (piezo: automated piezopipetting, n = 4) and the controls (man: manual pipetting, n = 3) were very similar. Almost all VEGF was released with the initial burst (93% within 2 h). No VEGF was released from the negative control (nc; n = 1).

Executive summary

- Macroscopic extrusion-based 3D printing (3D plotting) was combined with precise microdispensing of liquids enabling localized functionalization of 3D scaffolds during their fabrication.
- By broadening the range of applicable materials and their combinations, the potential for the fabrication of patient individual implants and complex tissue equivalents is enhanced.
- A fluorescein gradient on a 3D scaffold was accomplished by alternating extrusion of calcium phosphate cement strands and pipetting in a layer-by-layer fashion demonstrating the feasibility of the new fabrication strategy.
- Though slower than inkjet printing, the integrated nanoliter pipetting offers the possibility of dispensing an arbitrary number of different liquids on the same scaffold.
- Release kinetics of VEGF was not altered by using piezoelectric pipetting.
- Loading and cell seeding strategies need to be further investigated on the basis of agent–solution/material and cell/material interaction, respectively, to achieve effective local functionalization and good cell adhesion.

Acknowledgements

The authors would like to thank S Brüggemeier for excellent technical assistance.

Financial & competing interests disclosure

The authors thank the Saxon Ministry for Higher Education, Research and the Arts (SMWK, contract No. 4–7531.60/29/24) for financial support. The authors have no other relevant affiliations or financial involvement with any organization or entity with a financial interest in or financial conflict with the subject matter or materials discussed in the manuscript apart from those disclosed.

No writing assistance was utilized in the production of this manuscript.

References

1 Ferris CJ, Gilmore KJ, Wallace GG, in het Panhuis M. Biofabrication: an overview of the approaches used for printing of living cells. *Appl. Microbiol. Biotechnol.* 97(10), 4243–4258 (2013).

2 Derby B. Printing and prototyping of tissues and scaffolds. *Science* 338(6109), 921–926 (2012).

3 Billiet T, Vandenhaute M, Schelfhout J, Van Vlierberghe S, Dubruel P. A review of trends and limitations in hydrogel-rapid prototyping for tissue engineering. *Biomaterials* 33, 6020–6041 (2012).

4 Lode A, Meissner K, Luo Y *et al.* Fabrication of porous scaffolds by three-dimensional plotting of a pasty calcium phosphate bone cement under mild conditions. *J. Tissue Eng. Regen. Med.* 8(9), 682–693 (2014).

5 Kolesky DB, Truby RL, Gladman AS, Busbee TA, Homan KA, Lewis JA. 3D bioprinting of vascularized, heterogeneous cell-laden tissue constructs. *Adv. Mater.* 26, 3124–3130 (2014).

6 Vorndran E, Geffers M, Ewald A, Lemm M, Nies B, Gbureck U. Ready-to-use injectable calcium phosphate bone cement paste as drug carrier. *Acta Biomater.* 9, 9558–9567 (2013).

7 Akkineni AR, Luo Y, Schumacher M, Nies B, Lode A, Gelinsky M. 3D plotting of growth factor loaded calcium phosphate cement scaffolds. *Acta Biomater.* 27, 264–274 (2015).

8 Heinemann S, Roessler S, Lemm M, Ruhnow M, Nies B. Properties of injectable ready-to-use calcium phosphate cement based on water-immiscible liquid. *Acta Biomater.* 9(4), 6199–6207 (2013).

9 McKinney RM, Spillane JT, Pearce GW. Fluorescein diacetate as a reference color standard in fluorescent antibody studies. *Anal. Biochem.* 9(4), 474–476 (1964).

10 Kimball S, Mattis P, GIMP-Team. GNU Image Manipulation Program. (1998–2014). www.gimp.org

11 Knaack S, Lode A, Hoyer B *et al.* Heparin modification of a biomimetic bone matrix for controlled release of VEGF. *J. Biomed. Mater. Res. Part A* 102(10), 3500–3511 (2014).

12 Ahlfeld T, Akkineni AR, Förster Y *et al.* Design and fabrication of complex scaffolds for bone defect healing: combined 3D plotting of a calcium phosphate cement and a growth factor-loaded hydrogel. *Ann. Biomed. Eng.* doi:10.1007/s10439–016–1685–4 (2016) (Epub ahead of print).

13 Gasperini L, Maniglio D, Motta A, Migliaresi C. An electrohydrodynamic bioprinter for alginate hydrogels containing living cells. *Tissue Eng. Part C* 21(2), 123–132 (2014).

14 Schütz K, Placht AM, Paul B, Brueggemeier S, Gelinsky M, Lode A. 3D plotting of a cell-laden alginate/methylcellulose blend: towards biofabrication of tissue engineering constructs with clinically relevant dimensions. *J. Tissue Eng. Regen. Med.* doi:10.1002/term.2058 (2015) (Epub ahead of print).

15 Landers R, Muelhaupt R. Desktop manufacturing of complex objects, prototypes and biomedical scaffolds by means of computer-assisted design combined with computer-guided 3D plotting of polymers and reactive oligomers. *Macromol. Mater. Eng.* 282, 17–21 (2000).

16 Jonczyk R, Timur S, Scheper T, Stahl F. Development of living cell microarrays using non-contact micropipette printing. *J. Biotechnol.* 217, 109–111 (2016).

17 Lode A, Reinstorf A, Bernhardt A, Wolf-Brandstetter C, Koenig U, Gelinsky M. Heparin modification of calcium phosphate bone cements for VEGF functionalization. *J. Biomed. Mater. Res. Part A* 86(3), 749–759 (2008).

REVIEW

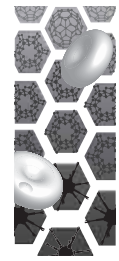

3D polymer scaffolds for tissue engineering

K Seunarine[1†], N Gadegaard[1], M Tormen[2], DO Meredith[1], MO Riehle[1] & CDW Wilkinson[1]

[†]Author for correspondence
[1]University of Glasgow Centre for Cell Engineering, Glasgow G12 8QQ, UK
Tel.:+44 141 330 6126
E-mail:ks@elec.gla.ac.uk
[2]TASC Laboratory of the Istituto Nazionale della Fisica della Materia, S.S.14 km. 163,5, I-34012, Basovizza-Trieste, Italy

This review discusses some of the most common polymer scaffold fabrication techniques used for tissue engineering applications. Although the field of scaffold fabrication is now well established and advancing at a fast rate, more progress remains to be made, especially in engineering small diameter blood vessels and providing scaffolds that can support deep tissue structures. With this in mind, we introduce two new lithographic methods that we expect to go some way to addressing this problem.

In the USA, more than 6000 people die each year as a result of the shortage of donor organs. In 1990, the difference between the number of organs donated and the number of patients waiting for organs was 9000; todays it is over 55,000 [101]. Tissue engineering (TE) is seen by many as the only way to address this shortage.

TE is an interdisciplinary field that draws from materials science, cell biology, biotechnology and chemistry to synthesize effective strategies for the repair or replacement of damaged or diseased tissues [1]. Artificially engineered scaffolds are a key requirement in TE. The fundamental requirements of these scaffolds are that they: provide mechanical support, are biocompatible, degrade over a predetermined period of time, can be moulded into the desired shape, are easy to sterilize and allow cell attachment and migration; however, many scaffold-based TE approaches are still experimental, therefore it is not yet clear what defines a so-called 'ideal scaffold' [2]. What is known is that 'ideal' scaffolds are likely to be different for each tissue type. Scaffolds must mimic, as far as possible, the structure and biological function of the extracellular matrix (ECM). They must also support expanded autologous cells as they proliferate and secrete their own ECMs, thus replacing the biodegradable scaffolds as the tissues grow.

Laboratory expanded skin cells are now provided by CellTran Ltd (UK) for wound healing in patients with extensive burns and chronic wounds. Cartilage is another tissue that is grown routinely by Mercy Tissue Engineering (Australia) to provide cartilage for knee implants. Skin and cartilage are two of the most common tissues grown under laboratory conditions. The main reason for this is that cartilage does not require blood vessels or nerves and skin is sustained by the nutrients that diffuse through the thickness of cells that make up the graft.

Attempts have been made to grow more biologically challenging organs *in vivo*. In one recently publicized case, Atala and colleagues used autologous bladder muscle and urothelial cells to grow functioning bladders that were transplanted back into the patients' bodies.

The autologous cells were expanded *in vivo* before attaching them to scaffolds. He used two different scaffold materials, one made of decellularized bladder submucosa and the other made from collagen and polyglycolic acid (PGA). The exterior surface of the scaffold was seeded with smooth muscle cells before the inside of the scaffolds were seeded with urothelial cells. The engineered bladders were ready to be implanted within only 7–8 weeks of the biopsy to harvest the cells [3].

This review summarizes some of the most recent state-of-the-art techniques for fabricating scaffolds for TE. Many of these scaffolds have already been used to grow functioning tissues, although the lack of controlled internal channels inhibits the viability of cells deep within the scaffold. Therefore, we describe the development of our lithographically defined structures for producing scaffolds that incorporate blood vessel architectures and scaffolds for vascular TE.

Scaffold fabrication technologies

In this review, we focus on four groups of methods of fabricating scaffolds: scaffold moulding, electrospinning, solid freeform fabrication (SFF) and casting and lithographic techniques.

Keywords: lithography, scaffolds, tissue engineering

future medicine

Figure 1. Salt leaching.

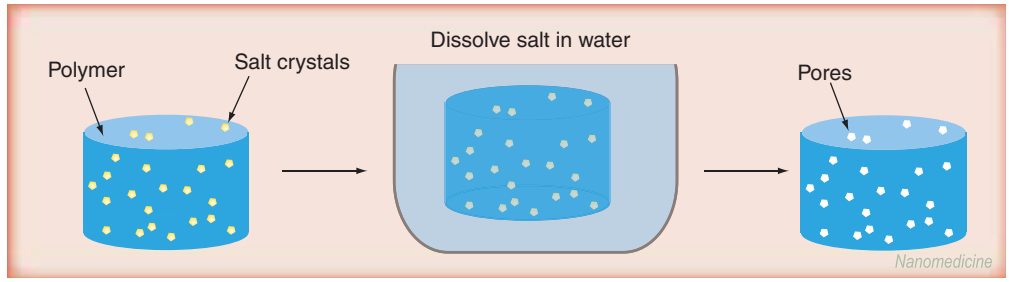

A polymer solution containing dispersed water-soluble NaCl is moulded into a suitable shape. The salt particles are then dissolved in water to leave open pores in the polymer structure.

Scaffold moulding

Solvent casting/melt-moulding & particulate leaching

A high molecular weight polymer solution in an organic solvent – typically chloroform or methylene chloride (MC) – containing dispersed water-soluble salt (NaCl) particles is precipitated into an excess of nonsolvent. The polymer–salt composite is then processed by thermal processing methods into devices of various shapes and sizes. The NaCl particles are then dissolved in water to leave a porous structure (Figure 1).

The porosities of the scaffolds can be varied between 70 and 95% by adjusting the polymer:salt ratio and the pore sizes of 100–500 µm can be controlled by independently varying the leachable particle size [4–6].

Other porogens (i.e., labile pore-generating materials) have been used, including spheres of paraffin [7] and crystals of saccharose [8]. Zhang and colleagues reported better pore connectivity with spherical porogens than cubic ones. Scaffolds that are made from NaCl porogens can lead to a dispersed distribution of interconnectivity, since two or more adjacent cubic particulates may merge into one large pore, while two spherical porogens always lead to two macropores. They also found that, as the porosity increased above 95%, most of the cubic-pore scaffolds collapsed during salt leaching, but the spherical ones still kept their shape and integrity.

Thomson and colleagues found that high porosities (>58%) could not be achieved with gelatine porogens because weight fractions above 45% resulted in swelling during the leaching process, which led to rupturing of the foam structure [9].

One of the biggest disadvantages with solvent casting and particulate leaching is the organic solvents that are difficult to remove fully. These solvents are usually harmful to cells. Several authors, including Mikos and colleagues [10], have proposed melt-moulding as a means of circumventing the problems associated with solvent casting. Melt-moulding involves premixing polymer powder with the solid porogen before the mixture is hot-pressed into a mould. The porogen is then leached as described previously.

Reignier and colleagues have produced interconnected pores by combining selective polymer leaching in a co-continuous blend and salt particulate leaching. A co-continuous blend of polycaprolactone (PCL) and polyethylene oxide (PEO) and NaCl particles were melt blended. Extraction of the continuous PEO and NaCl using water as a selective solvent yielded highly porous (75–88%) PCL scaffolds with fully interconnected pores. The explanation for the open-pore structure is that the NaCl particles and co-continuous polymer blend give very different pore sizes with bimodal pore size distributions [11].

Figure 2. Polymer disks are saturated with an inert gas.

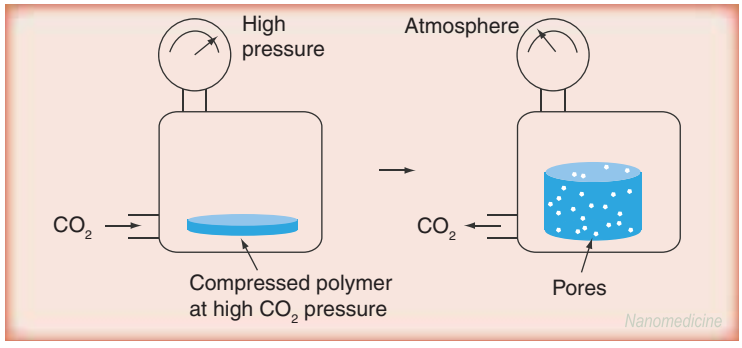

A rapid reduction in pressure results in nucleation and formation of bubbles in the polymer.

Figure 3. Emulsification.

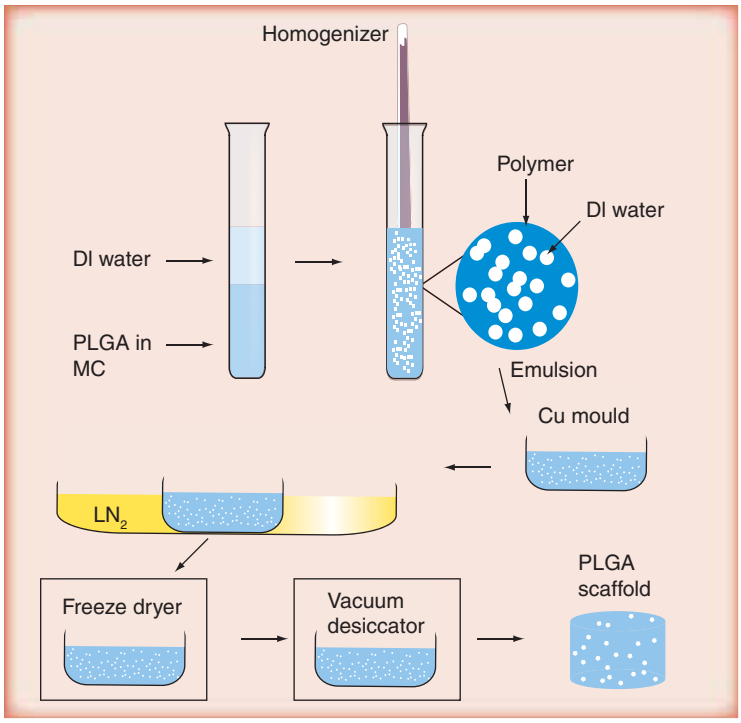

Deionized water is added to a solution of polymer and methylene chloride. The polymer solution is then moulded and freeze dried to remove the water and solvent.
DI: Deionized; MC: Methylene chloride; PLGA: Poly(lactic-*co*-glycolic acid).
Adapted from [22] ©1995 with permission from Elsevier.

Gas foaming

Gas foaming was developed originally as an alternative to particulate leaching methods in order to overcome the need to use organic solvents during casting of the polymer material. It relies on supercritical fluid (a substance above its critical temperature [Tc] and critical pressure [Pc]) foaming to produce the porous scaffolds (Figure 2).

Mooney and colleagues used gas as a porogen in order to eliminate the use of these organic solvents during the fabrication process [12] – gas foaming uses inert gas, typically CO_2 or N_2, to form the pores. In this process, disks of polymer, typically poly(L-lactic acid) (PLLA), PGA or poly(lactic-*co*-glycolic acid) (PLGA), were exposed to high-pressure CO_2 for a number of hours or even days in order to achieve saturation. Subsequent rapid reduction in pressure, down to atmospheric pressure, causes the nucleation and formation of pores in the polymer matrix from the CO_2 gas [13]. The pores obtained with this technique were largely unconnected. Lips and colleagues produced closed cell foams (i.e., foams with unconnected pores) in polyimide with maximum porosities of approximately 90% and various pore sizes, ranging from 2.5 to 100 µm [14].

Early gas foaming methods required high temperatures to make the polymer disks, thus prohibiting the incorporation of cells or bioactive molecules. Quirk and colleagues used supercritical fluid (CO_2) processing methods to allow fabrication of porous scaffolds without organic solvents or high temperatures [15]. This gives tissue engineers the ability to incorporate delicate biological molecules into the scaffold.

One of the main problems with porous scaffolds is the lack of interconnected pores. A technique that combines salt leaching and gas foaming has been shown to produce interconnected pores [16].

Nam and colleagues used gas foaming and particulate leaching to produce open pore structures [17]. Ammonium bicarbonate was added to a polymer solution before the solvent was evaporated. The structure was then immersed in water. Immersion in water resulted in concurrent gas evolution and particulate leaching, giving porosities of up to 90% and pore sizes of 200–500 µm.

Open pores have also been produced by Kim and colleagues, who used a modified water-in-oil-in-water ($W_1/O/W_2$) double emulsion solvent evaporation method to produce microspheres. The incorporation of an effervescent salt, ammonium bicarbonate, in the primary W_1 droplets produced CO_2 and ammonia gas bubbles spontaneously during the solvent evaporation process, which created well interconnected pores in the resultant microspheres [18].

Phase separation & emulsification

Phase separation uses differences in solvent partitioning between polymer rich and polymer poor phases to form porous scaffolds. There are several methods of inducing phase separation in mixtures of such polymers.

Liquid–liquid phase separation uses thermodynamic principles to create polymer-rich and -poor phases within a polymer solution. The polymer-poor phase is then dissolved in a solvent to leave a porous polymer structure. Bioactive molecules can also be incorporated into the scaffold structure by dissolving or dispersing them in the polymer solution. As the scaffold degrades, the bioactive molecules are delivered to cells within or surrounding the scaffold [19].

Both PLLA and PLGA scaffolds have been made using the phase separation technique [20]. More recently, Yang and colleagues designed and fabricated porous PLLA and PLGA scaffolds

Figure 4. Electrospinning apparatus setup.

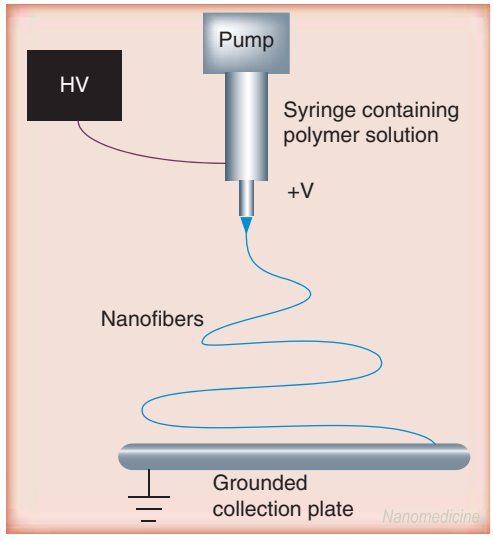

The HV supply is typically 10 kV, the distance between the needle and collection plate is 4–10 cm and the flow rate is 0.03 ml/min [25,26].
HV: High voltage.

with oriented microtubules using a modified temperature-induced phase separation technique with a dioxane solvent and a controlled thermal gradient. The carefully controlled thermal gradient and super cooling temperature allowed them to manufacture orientation-structured microtubule-like pores with diameters ranging between 40 and 240 µm [21].

Figure 5. Laser sintering.

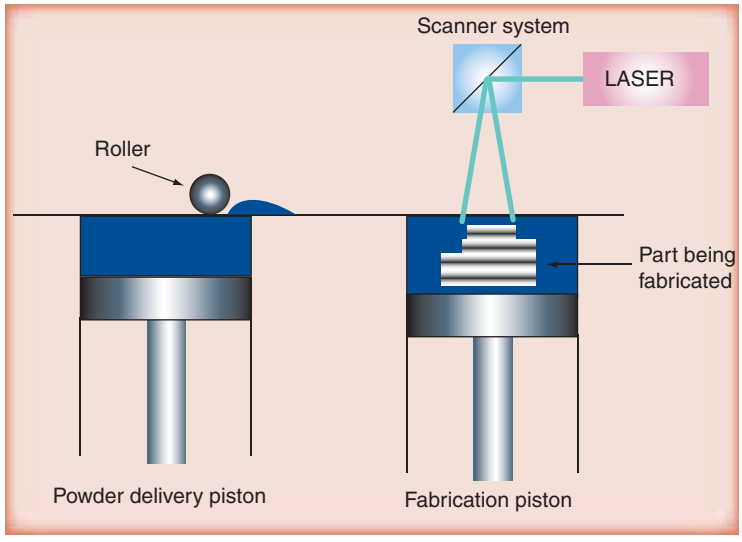

The fabrication piston is lowered according to the layer thickness.
Adapted from [102]. Worldwide Guide to Rapid Prototyping web-site©.

Porous scaffolds that are made using emulsion freezing are fabricated as follows:

- A synthetic polymer is dissolved in a suitable solvent
- Water is added to the solution and the two liquids mixed in order to obtain an emulsion
- The solution is then moulded and frozen before the two phases can separate
- Freeze drying removes the dispersed water and solvent leaving a solidified, porous polymer structure (Figure 3)

Scaffolds with porosities of 95% and median pore sizes of 13–35 µm have been made using this technique [22].

Emulsification has been used to create spherical porogens from gelatin. Liu and colleagues developed a one-step process to fabricate surface-modified nanofibrous PLLA scaffolds. First, gelatin spheres with smooth surfaces were prepared by nonsurfactant emulsification, solvent extraction and freeze drying. The sphere sizes ranged from 100 to 600 µm, with a maximum yield at approximately 300 µm. A 3D nanofibrous PLLA scaffold was then fabricated using gelatin spheres as a porogen. Gelatin molecules were entrapped onto the scaffold surface during the fabrication process. The scaffolds were then immersed in distilled water at 40°C with magnetic stiring to leach out the gelatin spheres. Fiber diameters ranged from 50 to 500 nm, which is on the same scale as natural collagen fiber bundles [23].

Electrospinning

Nonwoven fabrics consisting of extremely fine polymer fibers are produced through a process known as electrospinning. The process involves the application of a high electrostatic field to a capillary connected to a syringe containing a polymer solution. A pendant droplet of the polymer solution at the capillary tip is deformed into a conical shape, known as a Taylor cone. When the voltage exceeds a threshold, electrostatic forces overcome surface tension and a fine charged jet is ejected. The solvent in the ejected jet begins to evaporate to form polymer fibers that travel toward a grounded counter electrode where they are collected. A typical electrospinning setup is shown in Figure 4 [24].

A wide variety of materials, such as polystyrene (PS), polymethyl methacrylate (PMMA), hyaluronic acid, PCL and polyurethane (PE), have been used in electrospinning [25–28]. Electrospinning can produce polymer fibers with diameters ranging from several microns to 100 nm or

Figure 6. Schematic illustration of a typical drop-on-demand printing system.

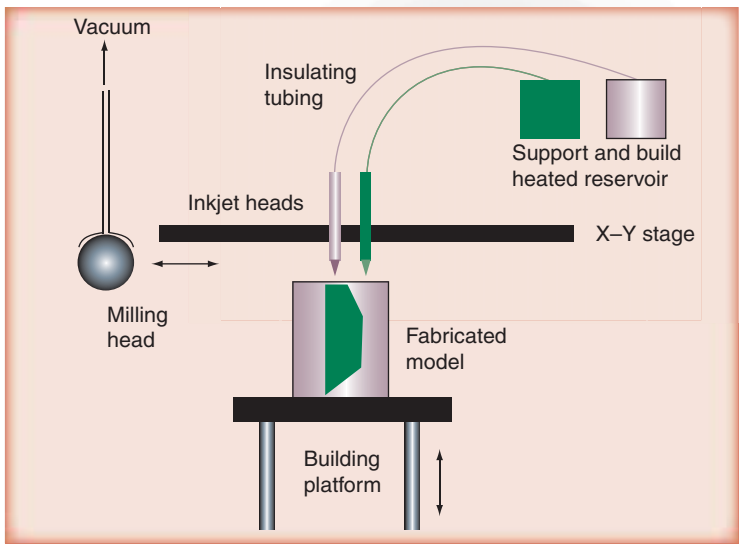

The milling head levels the surface before the next layer is deposited. Adapted from [39] ©2006 with permission from Elsevier.

less [29]. However, it is difficult to make a scaffold possessing pore sizes that are appropriately large for cells [30]. Vaz and colleagues made tubular scaffolds for blood vessels using a multilayering electrospinning technique. His scaffolds consisted of a stiff and oriented polylactic acid (PLA) fibrous layer on the outer surface and a pliable and randomly oriented fibrous PCL layer on the inner surface. A rotating mandrel collector was used to gather fibers sequentially, that is, first PCL and then PLA. The spinning conditions were chosen through careful selection of solvent, polymer concentration, voltage, air gap, flow rate, spinning time and mandrel rotation speed. The rotation speed was increased for PLA in order to create an oriented outer layer [31].

Solid freeform fabricated scaffolds & casting

SFF is a method of rapid prototyping that is used to build 3D scaffolds layer by layer, through material deposition on a stage by computer control using digital models. Those digital models come from computer-aided design modeling, 3D reconstruction of computed tomography/magnetic resonance imaging (CT/MRI) images [32].

Selective laser sintering

The selective laser sintering technique uses a CO_2 (infrared) laser beam to sinter thin layers of powdered polymetric material to form a solid 3D object. The laser beam raises the powder temperature to the point of melting and causes the particles to be fused together to form a solid mass. Subsequent layers are built directly on top of the previously sintered layer (Figure 5). The smallest attainable feature is determined by the powder particle size [33]. Williams and colleagues report that the optimum particle size for selective laser sintering is 10–100 µm. Particles smaller than 10 µm exhibit poor flow and spreading properties as well as sintering much faster when trapped in pores and feature boundaries – this causes inaccuracies in feature dimensions as well as making it harder to remove excess powder from the pores and boundaries. Larger particles increase the granularity of edges, surfaces and layers. Commercial selective laser sintering machines typically produce focused laser spots of approximatley 450 µm, which clearly limits the smallest processed feature [34].

Ink jet printing (adhesion bonding) & fused deposition modeling

Three-dimensional printing (3DP™) was developed originally at the Massachusetts Institute of Technology, USA, as a means of creating complex shapes to emulate the tissue that the scaffold is designed to repair or replace [13]. 3D structures are created by inkjet printing liquid binder to join loose powder in successive 2D slices [35]. The liquid solvent binder can be printed onto a powder bed of porogens and polymer particles; however, the size distribution of the porogens places a limit on the minimum incremental layer thickness. Kim and colleagues have combined 3DP with salt leaching to

Figure 7. Illustration of the type of 0/90° honeycomb structure produced by fused deposition modeling.

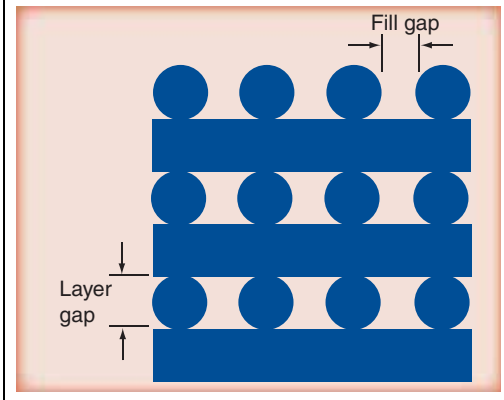

Adapted from [40] ©2002 with permission from Elsevier.

Figure 8. Stereolithography apparatus.

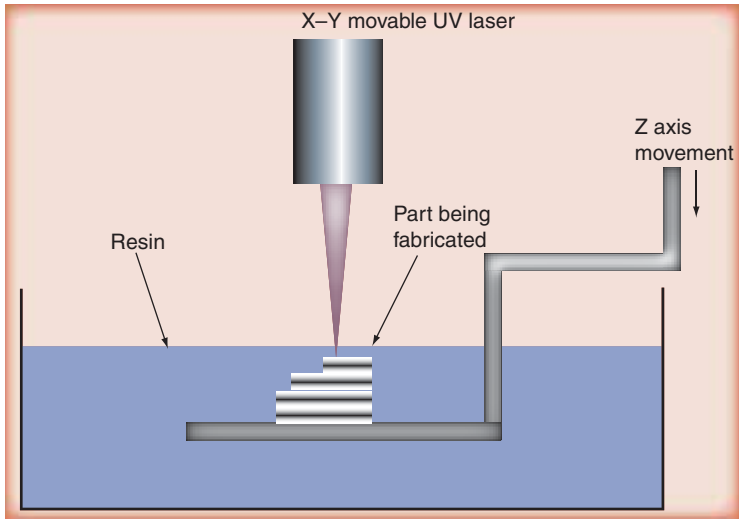

Adapted from [42] ©2004 with permission from Elsevier.

achieve interconnected pore channels of approximately 800 µm, with microporosities of 45–150 µm [36].

Lee and colleagues fabricated scaffolds with 300–500 µm interconnected pores using an indirect 3DP approach, where the mould was first printed before the polymer material was cast into the mould cavity. He fabricated moulds for villi-containing scaffolds in a commercially available plaster powder with an average diameter of approximately 20 µm. During printing, a 100-µm layer of this powder was spread and the binder was printed to selectively form the 2D pattern. The process was repeated layer by layer until the structure was completed. After drying, the plaster mould was infiltrated with polyethylene glycol (PEG) to fill out the surface pores and enhance mould strength for subsequent processing. PLGA (15%, w/w), chloroform and methanol (67/33, w/w), and sucrose particles (100–150 µm diameter) were mixed and cast into the moulds. The scaffolds were then dried and the solvent removed by freeze drying. The mould and sucrose porogen were removed simultaneously by immersing the scaffolds in deionized water [37].

Toboas and colleagues also used indirect SFF by coupling SFF with conventional sponge fabrication procedures. They used phase separation and emulsion–solvent diffusion, followed by porogen leaching, to PLA scaffolds containing both computationally designed pores (500, 600 and 800 µm wide channels) with solvent-fashioned local pores (50–100 µm wide voids) [38].

Drop on demand printing (DDP) is a SSF technique capable of generating microscale physical features for TE scaffolds. Thermoplastic porogens with 100% connectivity were designed and fabricated using a commercially available DDP machine (Figure 6). The square voids in the thermoplastic porogen were then filled by injection moulding with either pure PCL or homogenous polymer–ceramic composites of PCL and calcium phosphate. The thermoplastic porogen was then removed by dissolution in ethanol to leave the PCL or PCL–CaP scaffold. Pore sizes as small as 200 µm were attainable using this indirect (porogen-based) method [39].

Fused deposition modeling (FDM) is an extrusion-based rapid prototyping technique that has been used to fabricate honeycomb-like structures with fully interconnected networks of pores. Zein and colleagues used bioabsorbable PCL microfilaments of 260–370-µm diameter to produce structures (Figure 7) with porosities of 48–77% and channel sizes of 160–700 µm [40]. FDM forms 3D objects from computer-generated models, in a similar way to the rapid prototyping methods described previously. This system uses an extruder, which can move in the X–Y directions by computer control, to force out a thermoplastic filament and deposit the semi-molten polymer filament, layer by layer, onto a building platform. When a layer has been deposited, the building platform is lowered before deposition of the next layer begins.

Photopolymerization (stereolithography)

Stereolithography is based on the principle of photopolymerization of photopolymer resins that is initiated by the energy from incident electromagnetic radiation (typically ultraviolet [UV] radiation) [41]. Typical stereolithography apparatus (SLA) is illustrated in Figure 8. UV light from a laser is directed onto preprogrammed regions of a layer of liquid polymer, causing the exposed regions to solidify. The stage is then lowered so that the part is covered with a fresh layer of resin and the process repeated [42]. A common spot size used in SLA is 250 µm; this is a compromise between precision and writing speed [43].

Hydrogels are an important material in TE because it is possible to form these materials *in situ* by minimally invasive techniques, such as by injection. A number of hydrogel materials can be formed via photopolymerization processes and are mild enough to be carried out in the presence of living cells [44].

Figure 9. Process flow for making scaffolds made by solid freeform fabrication and casting.

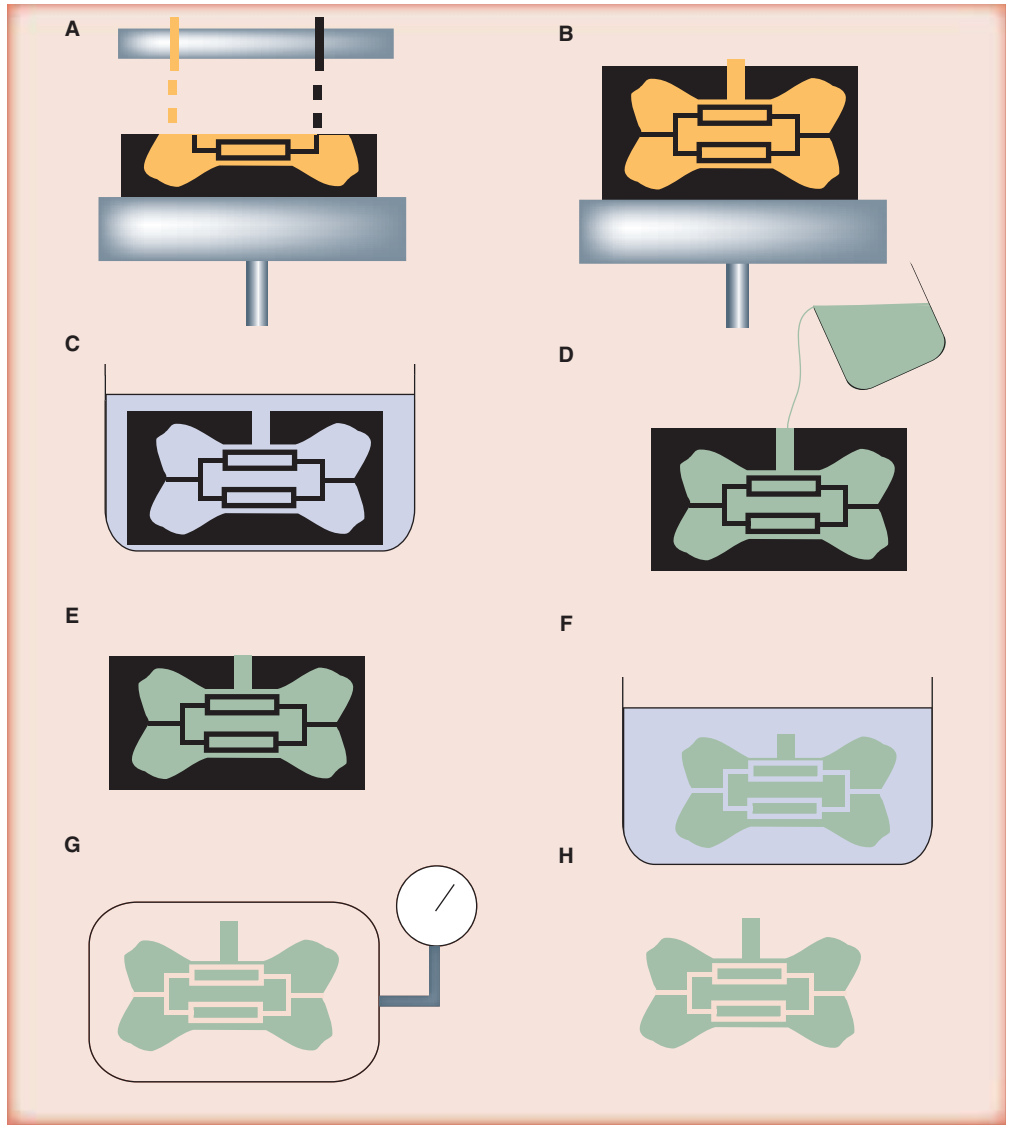

(A) Computer-controlled droplet deposition of the mould and support material to form a layer. **(B)** The building platform moves down for the next layer to be written. **(C)** Support material is removed by immersion in a selective solvent. **(D)** Collagen dispersion is cast into the mould. **(E)** Collagen dispersion is frozen at -20°C. **(F)** Mould is dissolved in ethanol. **(G)** Collagen scaffold is dried in a critical point drier.
Adapted with kind permission of reproduction from *European Cells and Materials* (ecmjournal.org) [51].

Casting

Tubes are an important concept in TE as the development of a small-diameter blood vessel substitute is required for vascular TE. One of the biggest issues is providing vessels that resist platelet adhesion and promote endothelialization.

Polytetrafluoroethylene (PTFE) and polyethylene terephthalate (PET) have been used successfully in treating the pathology of large-diameter arteries (>6 mm, inner diameter), although no materials have been proven to be successful in replacing small diameter blood vessels (<6 mm). The main reason for the long-term failure of the small-diameter vascular graft is the incomplete cover of endothelial cells on the vascular graft surfaces [45].

Goodman and colleagues demonstrated a multistep technique for growing small-diameter blood vessels using arteries and veins of 1–4 mm internal diameter from several mammalian species. A

syringe was used to fill and distend cannulated blood vessels to their *in vivo* states using a buffer solution. Replicas of the subendothelial ECM surfaces of the denuded and distended vessels were prepared by casting the lumenal space with a methacrylate resin. The vascular tissue was then removed by maceration in KOH. Following rinsing and drying, the replica was dipped into PE a number of times to provide a 10–15-µm thick PE film. The methacrylate negative casts were then removed by solvation in acetone to expose the luminal replica surfaces [46].

Wu and colleagues have also attempted to fabricate small-diameter tubes (amongst other structures) using a room-temperature injection moulding/particulate leaching technique.

Figure 10. Schematic illustration of the fabrication procedure.

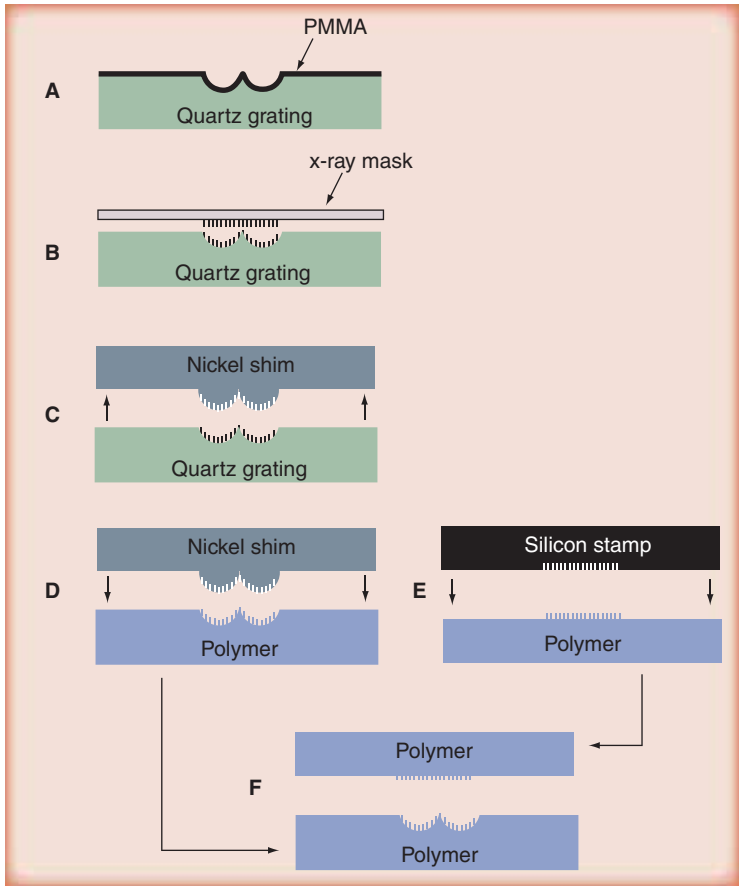

(A) A quartz master is coated with PMMA **(B)** The nanostructure is defined in the PMMA by x-ray lithography. **(C)** After development, a nickel shim is made from the 3D nanopatterned polymer structure. **(D)** The nickel shim is used to prepare many replicas in a biodegradable polymer. **(E)** A silicon stamp is used to emboss a flat nanoarray in other biodegradable polymer substrates. **(F)** The tubular scaffold is assembled by bonding the two substrates together.
PMMA: Polymethyl methacrylate.
Adapted from [55].

A polymer (PLGA or PCL) was dissolved in chloroform to obtain a polymer solution. Sieved NaCl particulates were then added to obtain a composite of particulate–polymer–solvent. The soft paste-like composite was then injected into a mould to produce the desired shape scaffold. In the case of the small-diameter tube, a small rod inside the mould determined the inner diameter of the tube [47]. Wu and colleagues cited outer diameters of 7 mm and a wall thickness of 1 mm, which implies inner diameters of 5 mm. No mention is made of biological investigations with these scaffolds, therefore it remains to be seen whether the technique can be used to grow small diameter vessels successfully.

Vozzi and colleagues used a polydimethylsiloxane (PDMS) mould – taken from patterned photoresist – to demonstrate three distinct methods of scaffold fabrication by soft lithography. Micromoulding involved coating the PDMS mould with PLGA, placing it under a vacuum to allow the polymer to fill the micromould and allow it to outgas. The excess PLGA was removed by dragging the edge of a glass slide across the top of the mould. The PLGA was then baked before being removed with a pair of tweezers. Microfluidic moulding was the second technique reported. In this method, the PDMS was used to form microfluidic channels by sealing the mould against a flat substrate. The PLGA solution was forced to flow through the channels by applying a negative pressure. When the channels were filled, the whole assembly was heated. When cooled, the PDMS was removed leaving the PLGA structure firmly attached to the rigid substrate. Spin-coating was the third and final variation of the method. In this case, the PDMS mould was spin-coated with PLGA and the solvent was then evaporated at room temperature. The scaffolds where then removed with a pair of tweezers. In order to make 3D scaffolds, the PLGA membranes were stacked together under an optical microscope and then laminated together. Vozzi and colleagues remark that, in the future, these techniques can be used to study the effect of scaffold architecture on cellular activities, such as proliferation, differentiation and motility [48]. The authors suggest that this novel technique may benefit from the PDMS moulds being made using the lithographically defined structures described later.

Synthetic polymer scaffolds produce a high local concentration of acidic by-products during degradation, which can induce an adverse inflammatory response [49]. Thus, Sachlos argues that collagen may be a more suitable scaffold material, primarily because it is the major constituent of ECM [50].

Figure 11. Scanning electron micrograph of the square array of circular Au absorbers on the x-ray mask.

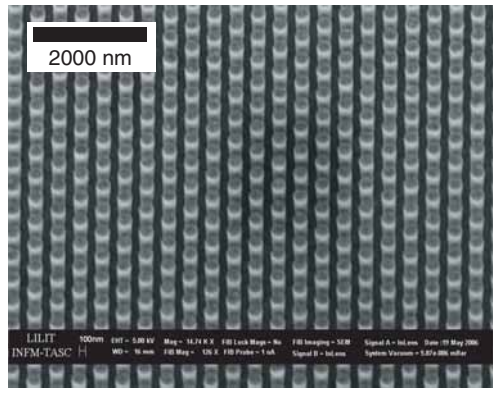

We have seen previously that a number of techniques have been combined to obtain scaffolds with more suitable physical and chemical characteristics for TE [16,38]. Sachlos and colleagues made scaffold moulds using SFF techniques and then cast a dispersion of collagen into them before freezing. The process began by making a mould, using an ink-jet printing system comprising two print heads, each delivering a different material (ProtoBuild™ and ProtoSupport™; Solidscape, Inc.). The support material was then removed by immersing the scaffold in a proprietary solvent (BioAct™). A dispersion of collagen was then cast into the mould and frozen to -20°C in a commercial freezer. The mould was then immersed in ethanol to remove the mould material and the remaining collagen scaffold dried in a critical point drier (Figure 9). The resulting collagen blood vessel scaffolds were 2.2 mm in diameter, branching out to two 1.7-mm diameter vessels [51].

Lithographically defined scaffolds

Early scaffolds fabricated by methods, such as particulate leaching, contain pores that reflect the shape and size of the particulates used, although they do not allow for the predetermination of the internal scaffold architecture or pore connectivity [42]. It is this lack of interconnectivity and control of internal channels that inhibits cell viability deep within the scaffold as cells toward the center of any 3D tissue grown *in vitro* become starved of nutrients and suffer from problems associated with the build up of waste products.

SFF gives much better spatial control over scaffold architecture, but is limited to a few hundred microns resolution. Any smaller scale features require a combination of SFF with one of the aforementioned methods, for example particulate leaching [38]. The incorporation of microchannels in scaffolds may allow nutrients to be supplied and waste products removed via microfluidic networks.

In contrast to SFF, lithographically defined scaffolds use techniques developed for fabricating integrated circuits and, as such, enable the fabrication of scaffolds with much greater precision and resolution. State-of-the-art lithographic techniques even facilitate the fabrication features on the nanoscale. The main aim of micro- and nanofabricated polymer scaffolds is to provide structures with a predetermined internal topography to aid mass transport of oxygen and nutrients as the well as removal of waste products.

Previous experimental work has demonstrated that biological cells do not adhere to surfaces that are patterned with nanopits (or pillars) of 120-nm diameter and 200-nm height on a 300-nm center-to-center spacing, provided that the nanopits are arranged in a regular pattern [52]. Thus, this effect is used to selectively reduce adhesion on the walls of micro- and nanofabricated scaffold structures. It is for this reason

Figure 12. Scanning electron micrograph of the patterned curved surface.

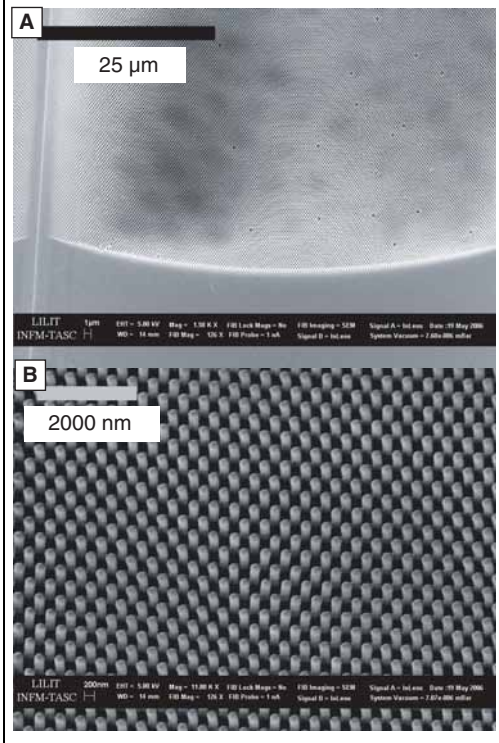

(A) Low magnification. **(B)** High magnification.

Figure 13. Double-sided embossing.

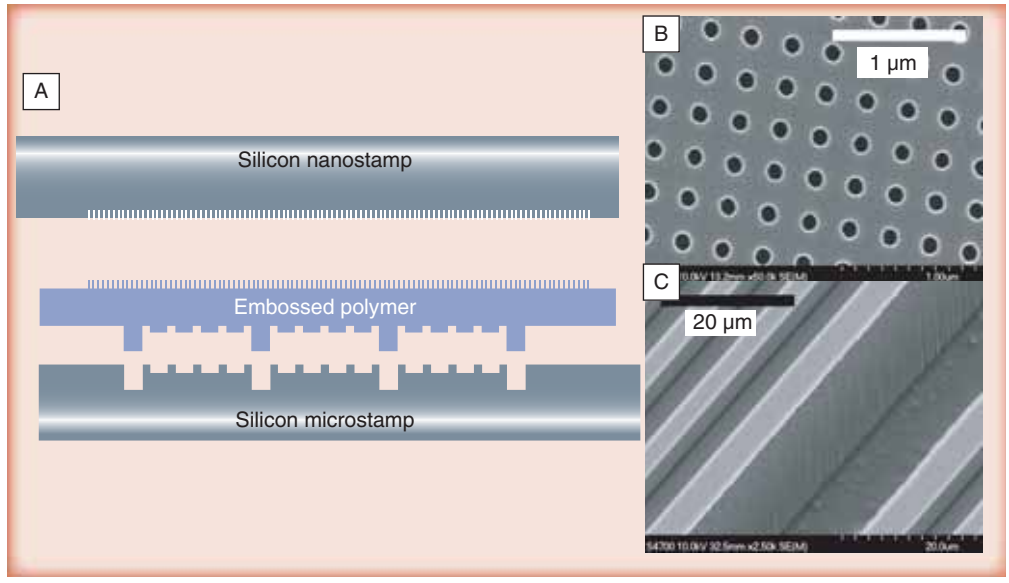

(A) Double-sided embossing schematic and scanning electron micrographs of the **(B)** nanostamp and **(C)** microstamp.

(performance and precision) that electron beam lithography (EBL) is used for pattern definition. EBL has some disadvantages in terms of cost and preparation time, but it is currently the only technique by which it is possible to control the lateral dimensions of features to less than 10 nm and with a position accuracy of approximately 1 nm. Even over large areas, several square centimeters, the precision of a state-of-the-art system is approximately 20 nm. Large areas of highly ordered arrays of nanopits or nanopillars are fabricated routinely using a high-speed patterning process, whereby the patterning time for 1 cm^2 of 1 billion features (~120 nm in diameter and spaced 300 nm apart) can be achieved in 1 h [53]. Using a conventional patterning approach, this would take more than 80 h. Two approaches that are currently under development are described below.

Approach I

There are a number of possible approaches to writing nanosized features onto 3D structures. Direct EBL has limitations in terms of its depth of focus, but this can be overcome, to some extent, by printing with x-rays onto a preformed substrate.

The method is outlined in Figure 10. First, a quartz substrate with a half-pipe profile is coated with a layer of PMMA resist. The PMMA resist is then exposed to x-ray photons through an x-ray mask. After exposure, the PMMA is developed and the substrate electroplated with nickel to form a stamp that is then used to melt-emboss a sheet of biodegradable polymer (PCL). Simultaneously, a nanopatterned silicon stamp is used to emboss a polymer lid in PCL (Figure 10E). The resulting curved and nanopatterned sheet of biodegradable polymer can then be formed into a tube by the addition of a nanopatterned lid.

An x-ray mask consisting of a square array of nanometric Au pillars (Figure 11) were used to pattern the PMMA resist (Figure 12). The printing of these very fine features using x-rays onto curved substrates coated in resist was limited by Fresnel diffraction of the beam. The realized size of the developed feature in resist depended on, among other parameters, the (varying) gap between the substrate and mask. The parameters of the x-ray exposure and amplitude of the quartz grating were chosen to give sufficient depth of focus [54]. We calculated a maximum gap of approximately 130 µm – the maximum distance between the mask and the bottom of the curved surface [55].

Approach II

Another method is being investigated for fabricating scaffolds with internal microchanneling. Thin sheets of polymer (~50 µm thick) were made by heating small sheets of PCL (~0.5 mm thick) to well above their melting temperature (>59°C) between two sheets of PTFE in a

Figure 14. Double-sided embossing.

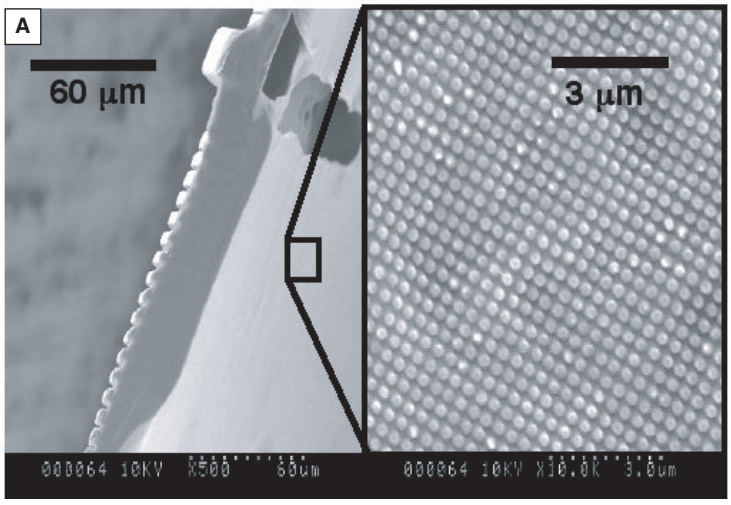

Cross section showing **(A)** micro-grooves and a spacer, **(B)** nanopillars on the underside.

hydraulic press (~1 ton), then cooling them back down to room temperature, before removing them from the press.

The thin sheets were then embossed on both sides – one side with microtrenches and spacers and the other with nonadhesive nanopillars/pits (Figure 13) [56]. The resulting film (Figure 14) was then rolled to form a structure that resembles a 'swiss roll' (Figure 15). Microtopographies are known to affect nearly all cell types [57], thus it is expected that the topography will guide cells into the structure.

Cell response

It is difficult to see cells in the middle of the 'swiss roll', so, in order to see the response of the cells to the structure, an embossed sheet (rolling up) was provided with a nanoembossed lid. This allowed easy observation of cell adhesion and alignment and the use of fluorescent agents to observe the cytoskeleton and growth. Thus, the initial 'swiss roll' design was transformed into a flat chamber, with grooves and spacers capped by a nanoembossed lid. For preliminary cell response studies, a human fibroblast cell line was used and seeded within the micro- and nano-topography chamber. At 48 h, cells were observed to have aligned with the grooved microtopography within the chamber. Their distribution within the structure showed that the cells were motile and exploring the structure. Intracellular labeling of the cytoskeleton components, actin (red) and tubulin (green) (Figure 16), demonstrate that the alignment to topographical features is found in these components as well as in the overall morphology.

Conclusions of our lithographic techniques

Approach I

X-ray lithography has been demonstrated successfully on curved surfaces, so the next stage of development will be to optimize the x-ray printing conditions to pattern the surface of a sufficiently deep curved surface with a regular array of nanopillars that will then be electroplated with nickel to make a durable stamp for embossing many sheets of PCL. Biological investigations remain to be carried out on these structures. It may be possible to use these structures together with some sort of inverse replica and casting technique, such as the one described by Goodman and colleagues, to create standalone scaffolds suitable for small-diameter blood vessels and capillaries. Alternatively, the two halves of the tube can be embossed on both sides to create a standard scaffold with internal microchannels.

Approach II

Currently, we are able to form thin double-sided embossed sheets using the techniques described. A tool has been constructed to allow the film to be rolled easily under constant tension before being secured at either end with surgical sutures. Preliminary cell response studies on

Figure 15. Embossed spacers are fabricated with separations set to give one spacer every 45° when the film is rolled up.

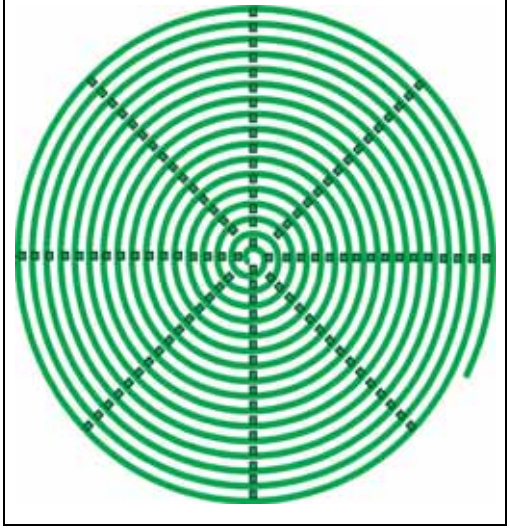

Figure 16. Fluorescent agents to show cytoskeleton and growth.

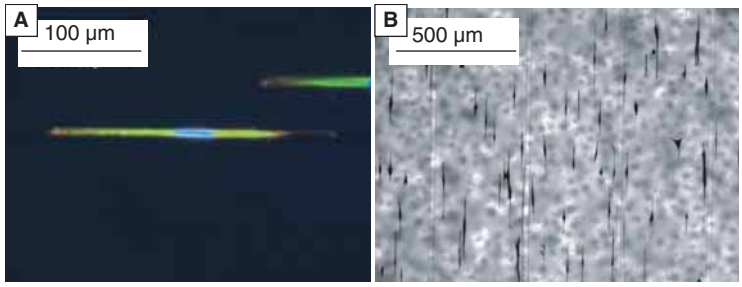

(A) Actin is red and tubulin is green. **(B)** Commasie blue staining shows the cells aligning to the microtrenches.

flattened versions of the 'swiss roll' scaffold have shown that human fibroblast cells align to the microgrooves and that they are motile and explore the structure. Cell viability deep within the structure is still an issue; this is thought to be a result of the lack of oxygen permeability. Investigations are underway currently to resolve this problem. One possible solution is to make holes in the polymer film before it is rolled.

Pore size and porosity of the material determine how easily cells can penetrate into the scaffold. The relative size distribution of pores and features produced in the most commonly used scaffolds is shown in Figure 17. From this, we see that casting gives the greatest range of sizes (from the nanoscale right up to centimer-scale dimensions); however, this technique does not tend to be suitable for mass production, especially Goodman's method of fabricating scaffolds for vascular tissues, which requires one donor vessel per scaffold produced (Table 1).

As mentioned previously, one of the fundamental requirements of TE scaffolds is that they provide sufficient mechanical support while the tissue is regenerating. Clearly, the mechanical strength required depends very much on the tissue that is being grown, which dictates what scaffolds and materials are available for supporting the growth of particular tissues and organs.

The dimensions in Table 2 give an idea of the relative strengths of the various scaffold types. It is clear that most, if not all, polymetric scaffolds are relatively weak when compared with traditional implant materials. In this case, electrospun fibers and some porous sponges tended to produce the weakest scaffolds of all of those reviewed. In particular, electrospun fibers can exhibit high tensile strengths, but scaffolds made from them are extremely weak in compression.

Conclusions & future perspective

The scientific and engineering communities are a long way off matching Nature in her ability to grow functioning tissues and organs. It is

Figure 17. A guide to the relative size distribution of features in the scaffolds discussed.

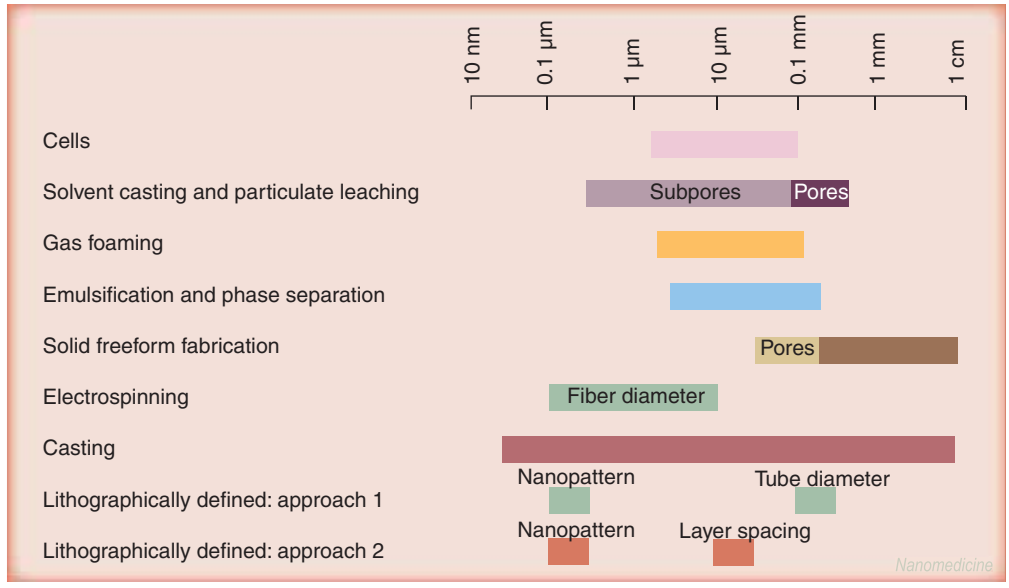

Table 1. Comparison of some of the main scaffold fabrication techniques reviewed.

Method of fabrication	Advantages	Disadvantages	Recently targeted tissues	Ref.
Salt leaching, gas foaming and phase separation	Easily controlled porosity Hybrid technique produces interconnected pores Allows incorporation of bioactive molecules for drug delivery	Residual solvents or high pressure Irregularly shaped pores/lack of interconnection and poor control over internal architecture	Bladder Cartilage Skin Bone Smooth muscle	[17, 58–61]
Electrospinning	High porosity. Extremely high surface-to-volume ratio	Poor mechanical strength Residual solvents Lack of control over microarchitecture	Heart Blood vessels Muscle Neural tissue Bone	[24,31, 62–65]
Solid free-form fabrication	Can produce complex shapes rapidly Good repeatability	Minimum feature size ~300 µm (direct SFF) Limited choice of photopolymerizable biomaterials Toxicity of binder material	Bone cartilage	[32,34, 39,66, 67]
Casting	Good replication of small diameter blood vessels	One donor vessel per scaffold	Blood vessels	[46]
Lithographically defined: approach I	Regular nanopatterns on nonflat surfaces Accurate control of feature dimensions and alignment of micro to nano Good repeatability	Maximum amplitude of micro surface is limited by x-ray lithography (~50 µm) Fresnel diffraction	Blood vessels	
Lithographically defined: approach II	Large 3D scaffold consisting of both micro- and nanostructures	Limited geometrical shapes. Permeability	Vascularized tissues for maximum fluid transport	

SFF: Solid freeform fabrication.

clear that a lot remains to be learned at all levels of TE; however, from an engineering point of view, the past 10 years has seen great advances in scaffold design. Starting with simple foams and fibers, it was quickly realized that connectivity between the pores, pore dimensions and properties of the scaffold materials are all of vital importance in facilitating cell seeding, migration, proliferation and the production of ECM. Significant advances have also been made in incorporating bioactive molecules into scaffolds. As more is learned about the behavior of cells on micro- and nanopatterned topographies, plasma and chemically treated surfaces, among others, future developments in scaffold fabrication technology are likely to be better tailored to produce designs and techniques that are targeted toward specific cell and tissue/organ types. Hybrid scaffold fabrication techniques have already been shown to be effective in pushing the limits of previously known techniques to meet the demands of more complex biological structures. One of the most pressing issues in current scaffold fabrication designs is the absence of vascularization; a strategy for addressing this is now of the utmost importance. Greater control of scaffold parameters will probably be just as important as vascularization in future scaffold designs. SFF has gained a lot of attention as it offers the ability to overcome some of the aforementioned control problems. It is unlikely that scaffolds will be custom built for individual patients because the cost will be prohibitive. The authors have pursued lithographic methods as a means of providing even more control, especially on the nanoscale, where cells are able to sense minute changes in surface topology. A big milestone will be the ability to fabricate structures with internal patterning on the nanoscale.

Acknowledgements

The partial support by the EC-funded project NaPa (contract no. NMP4-CT-2003–500120) is gratefully acknowledged. N Gadegaard is supported through a Royal Society of Edinburgh fellowship. The content of this work is the sole responsibility of the authors.

Table 2. A selection of yield strengths for a number of types of synthetic and biological materials.

Material	Strength	Ref.
Synthetic scaffolds		
Solid freeform fabrication (Selective laser sintering)	2.0–3.2 MPa (compressive yield strength)	[34]
Solid freeform fabrication (Fused deposition)	0.4–3.6 MPa (compressive yield strength)	[40]
Electrospinning (Various polymers)	~0.4 MPa 0.1–15 Mpa (tensile strength)	[25,29, 68–70]
Foam (Phase separation)	0.9 MPa (compressive yield strength)	[21]
Foam (Gas foaming and salt leaching of polyurethane urea modified with polyethylene glycol)	1.4 MPa (tensile strength)	[71]
Foam (Particulate leaching incorporating short hydroxyapatite fibers for reinforcement)	~2.82 MPa (compressive yield strength)	[9]
Foam (Particulate leaching with a hydrocarbon porogen)	Up to 5 MPa (compressive yield strength)	[72]
Implant materials		
Bioglass (45S5)	86–93 MPa (bending strength)	[73]
Hydroxyapatite	81–97 MPa (bending strength)	[73]
Titanium alloy (thermomechanically processed (Ti-35%Nb-4%Sn)	400–1000 MPa (tensile yield strength)	[74]
Stainless steel (X2CrNiMnMoN22136 for implant surgery)	500 MPa (min) (tensile yield strength)	[103]
Biological tissues		
Tendon (human patellar)	~58.7 MPa (tensile strength)	[75]
Trabecular bone (bovine tibia)	~19.7 MPa (compressive yield strength)	[76]

MPa: Megapascal.

Executive summary

- The literature reviewed suggests that there is not one scaffold that is 'ideal' for all tissue types.
- Interconnected pores are of vital importance for oxygen and media transport – poor scaffold porosity stunts cellularization toward the center of tissue constructs.
- Solvents and harsh processing conditions limit the use of some of the main scaffold fabrication techniques.
- Solid free-form fabrication gives much better spatial control over the scaffold architecture, but only within a few hundred microns.
- It is well known that cells respond to topographic cues both on the micro- and nanometric scale.
- Engineered organs are a long way off, although it appears likely that the construct will be patterned on both these scales.
- Lithographic techniques may be one way of achieving this.

Bibliography

1. Langer R, Vacanti J: Tissue engineering. *Science* 260, 920–926 (1993).
2. Hutmacher DW, Risbud V: Scaffold-based tissue engineering: rationale for computer-aided design and solid free-form fabrication systems. *Trends Biotechnol.* 22, 354–362 (2004).
3. Atala A, Bauer SB, Soker S *et al.*: Tissue-engineered autologous bladders for patients needing cystoplasty. *Lancet* 367, 1241–1246 (2006).
4. Katoh K, Tanabe T, Yamaguchi K: Novel approach to fabricate keratin sponge scaffolds with controlled pore size and porosity. *Biomaterials* 25(18), 4255–4262 (2004).
5. Freed LE, Marquis JC, Nohrla A *et al.*: Neocartilage formation *in vitro* and *in vivo* using cells cultured on synthetic biodegradable polymers. *J. Biomed. Mater. Res.* 27, 11–23 (1993).
6. Mikos AG, Wald HL, Sarakinos G *et al.*: Biodegradable cell transplantation devices for tissue regeneration. *MRS Symposium Proceedings* 252, 353–358 (1992).
7. Zhang JC, Wu LB, Jing DY *et al.*: A comparative study of porous scaffolds with cubic and spherical macropores. *Polymer* 46, 4979–4985 (2005).
8. Horak D, Kroupova J, Slouf M *et al.*: Poly(2-hydroxyethyl methacrylate)-based slabs as a mouse embyonic stem cell support. *Biomaterials* 25(22) 5249–5260 (2004).
9. Thomson RC, Yaszemski MJ, Powers JM *et al.*: Hydroxyapatite fiber reinforced poly(e-hydroxy ester) foams for bone regeneration. *Biomaterials* 19(21) 1935–1943 (1998).
10. Mikos AG, Thorsen AJ, Czerwonka LA *et al.*: Preparation and characterization of poly(L-lactic acid) foams. *Polymer* 35, 1068–1077 (1994).
11. Reignier J, Huncault MA: Preparation of interconnected poly(i-caprolactone) porous scaffolds by a combination of polymer and salt particulate leaching. *Polymer* 47, 4703–4717 (2006).
12. Mooney DJ, Baldwin DF, Suh NP *et al.*: Novel approach to fabricate porous sponges of poly(D,L-lactic-co-glycolic acid) without use of organic solvents. *Biomaterials* 17(14) 1417–1422 (1996).
13. Lanza RP, Langer R, Vacanti J: *Principles of Tissue Engineering (2nd Edition)*. Academic Press, CA, USA (2002).
14. Lips PAM, Velthoen IW, Dijkstra PJ *et al.*: Gas foaming of segmented poly(ester amide) films. *Polymer* 46, 9396–9403 (2005).
15. Quirk RA, France RM, Shakesheff KA *et al.*: Supercritical fluid technologies and tissue engineering scaffolds. *Curr. Opin. Solid State Mat. Sci.* 8, 313–321 (2004).
16. Harris LD, Kim BS, Mooney DJ: Open pore biodegradable matrices formed with gas foaming. *J. Biomed. Mater. Res.* 42, 396–402 (1998).
17. Nam YS, Yoon JJ, Park TG: A novel fabrication method of macroporous biodegradable polymer scaffolds using gas foaming salt as a porogen additive. *J. Biomed. Mater. Res.* 53, 1–7 (2000).
18. Kim TK, Yoon JJ, Lee DS *et al.*: Gas foamed open porous biodegradable polymetric microspheres. *Biomaterials* 27(2), 152–159 (2006).
19. Lo H, Ponticiello MS, Leong KW: Fabrication of controlled release biodegradable foams by phase separation. *Tissue Eng.* 1, 15–28 (1995).
20. Schugens C, Maquet V, Grandfils C *et al.*: Polyactide macroporous biodegradable implants for cell transplantation II. Preparation of polyactide foams for liquid-liquid phase separation. *J. Biomed. Mater. Res.* 30, 449–461 (1996).
21. Yang F, Qu X, Cui W *et al.*: Manufacturing and morphology structure of polyactide-type microtubules oreientation-structured scaffolds. *Biomaterials* 27(28), 4923–4933 (2006).
22. Whang K, Thomas CH, Healy KE *et al.*: A novel method to fabricate bioabsorbable scaffolds. *Polymer* 30(4), 837–842 (1995).
23. Liu X, Won Y, Ma PX: Porogen-induced surface modification of nano-fibrous poly(L-lactic acid) scaffolds for tissue engineering. *Biomaterials* 27(21), 3980–3987 (2006).
24. Yoshimoto H, Shin YM, Terai H *et al.*: A biodegradable nanofiber scaffold by electrospinning and its potential for bone tissue engineering. *Biomaterials* 24(12), 2077–2082 (2003).
25. Baker SC, Atkin N, Gunning PA *et al.*: Characterisation of electrospun polystyrene scaffolds for three-dimensional *in vitro* biological studies. *Biomaterials* 27(16), 3136–3146 (2006).
26. Piperno S, Lozzi L, Rastelli R *et al.*: PMMA nanofibers production by electrospinning. *Appl. Surf. Sci.* 252(15), 5583–5586 (2006).
27. Ji Y, Ghosh K, Shu XZ *et al.*: Electrospun three-dimensional hyaluronic acid nanofibrous scaffolds. *Biomaterials* 27(20), 3782–3792 (2006).
28. Williamson MR, Black R, Kielty C: PCL-PU composite vascular scaffold production for vascular tissue engineering: attachment, proliferation and bioactivity of human vascular endothelial cells. *Biomaterials* 27(19), 3608–3616 (2006).
29. Kidoaki S, Kwon IK, Matsudu T: Mesoscopic spatial designs of nano- and microfiber meshes for tissue-engineering matrix and scaffold based on newly devised multilayering and mixing electrospinning techniques. *Biomaterials* 26(1), 37–46 (2005).
30. Demir MM, Yilgor I, Yilgor E *et al.*: Electrospinning of polyurethane fibers. *Polymer* 43, 3303–3309 (2002).
31. Vaz CM, van Tuijl S, Bouten CVC *et al.*: Design of scaffolds for blood vessel tissue engineering using a multi-layering electrospinning technique. *Acta Biomater.* 1(5), 575–582 (2005).
32. Yan Y, Xiong Z, Hu Y *et al.*: Layered manufacturing of tissue engineering scaffolds via multi-nozzle deposition. *Zhang Materials Lett.* 57, 2623–2628 (2003).
33. Tan KH, Chua CK, Leong KF *et al.*: Scaffold development using selective laser sintering of polyetheretherketone-hydroxyapatite biocomposite blends. *Biomaterials* 24(18), 3115–3123 (2003).
34. Williams JM, Adewunmi A, Schek RM *et al.*: Bone tissue engineered using polycaprolactone scaffolds fabricated via selective laser sintering. *Biomaterials* 26(23), 4817–4827 (2005).
35. Lam C. XF, Mo XM, Teoh SH *et al.*: Scaffold development using 3D printing with a starch-based polymer. *Mater. Sci. Engin.* 20(1–2), 49–56 (2002).
36. Kim SS, Utsunomiya H, Koski JA *et al.*: Survival and function of hepatocytes on a novel three dimensional synthetic biodegradable polymer scaffold with an intrinsic network of channels. *Ann. Surg.* 228(1), 8–13 (1998).
37. Lee M, Dunn JCY, Wu BM: Scaffold fabrication by indirect three-dimensional printing. *Biomaterials* 26(20), 4281–4289 (2005).
38. Taboas JM, Maddox RD, Krebsbach PH *et al.*: Indirect solid freeform fabrication of local and global porous, biomimetric and composite 3D polymer-ceramic scaffolds. *Biomaterials* 24(1), 181–194 (2003).
39. Mondrinos MJ, Dembzynski R, Lu L *et al.*: Porogen-based solid freeform fabrication of polycaprolactone-calcium phosphate scaffolds for tissue engineering. *Biomaterials* 27(25), 4399–4408 (2006).
40. Zein I, Hutmacher DW, Tan KC *et al.*: Fused deposition modeling of novel scaffold architectures for tissue engineering applications. *Biomaterials* 23(4), 1169–1185 (2002).
41. Chua CK, Long KF: Rapid Prototyping: *Principles and Applications in Manufacturing*. Wiley, NY, USA (1997).

42. Tsang VL, Bhatia SN: Three-dimensional tissue fabrication. *Adv. Drug Deliv. Rev.* 56, 1635–1647 (2004).
43. Yang S, Leong K, Du Z *et al.*: The design of scaffolds for use in tissue engineering. Part II rapid prototyping techniques. *Tissue Eng.* 8, 1–11 (2002).
44. Nguyen KT, West JL: Photopolymerizable hydrogels for tissue engineering applications. *Biomaterials* 23(22), 4307–4314 (2002).
45. Ma Z, Kotaki M, Yong T *et al.*: Surface engineering of electrospun polyethylene teraphthalate (PET) nanofibers towards development of a new material for blood vessel engineering. *Biomaterials* 26(15), 2527–2536 (2005).
46. Goodman SL, Sims PA, Albrecht RM: Three-dimensional extracellular matrix textured biomaterials. *Biomaterials* 17(21), 2087–2095 (1996).
47. Wu L, Jing D, Ding J: A "room temperature" injection molding/particulate leaching approach for fabrication of biodegradable thee-dimensional porous scaffolds. *Biomaterials* 27(2), 185–191 (2006).
48. Vozzi G, Flaim C, Ahluwalia A *et al.*: Fabrication of PLGA scaffolds using soft lithography and microsyringe deposition. *Biomaterials* 24, 2533–2540 (2003).
49. Yaszemski MJ, Payne RG, Hayes WC *et al.*: Evolution of bone transplantation: molecular, cellular and tissue strategies to engineer human bone. *Biomaterials* 17(2), 175–185 (1996).
50. Sachlos E, Reis N, Ainsley C *et al.*: Novel collagen scaffolds with predefined internal morphology made by solid freeform fabrication. *Biomaterials* 24(8), 1487–1497 (2003).
51. Sachlos E, Czernuszka JT: Making tissue engineering scaffolds work. Review on the application of solid freeform fabrication technology to the production of tissue engineering scaffolds. *Eur. Cell Mater.* 5, 29–40 (2003).
52. Curtis A, Wilkinson CDW: Nanotechniques and approaches in nanobiotechnology. *Trends Biotechnol.* 19, 97–101 (2001).
53. Gadegaard N, Thoms S, Macintyre DS *et al.*: Arrays of nano-dots for cellular engineering. *Microelectronic Eng.* 67–68(1), 162–168 (2003).
54. Toyota E, Washio M: Extendibility of proximity x-ray lithography to 25 nm and below. *J. Vac. Sci. Techol.* B20(6), 2979–2983 (2002).
55. Seunarine K, Tormen M, Gadegaard N *et al.*: Progress towards tubes with regular nano-patterned inner surfaces. *J. Vac. Sci. Technol. B* (In Press) (2006).
56. Gadegaard N, Martines E, Riehle MO *et al.*: Applications of nano-patterning to tissue engineering. *Microelectronic Eng.* 83, 1577–1581 (2006).
57. Wilkinson CDW, Riehle M, Wood M *et al.*: The use of materials patterned on a nano- and micro-metric scale in cellular engineering. *Mat. Sci. Eng. C* 19, 263–269 (2002).
58. Pattison MA, Wurster S, Webster TJ *et al.*: Three-dimensional, nano-structured PLGA scaffolds for bladder tissue replacement applications. *Biomaterials* 26(15), 2491–2500 (2005).
59. Yoo HS, Lee EA, Yoon JJ *et al.*: Hyaluronic acid modified biodegradable scaffolds for cartilage tissue engineering. *Biomaterials* 26(14), 1925–1933 (2005).
60. Lee SB, Kim YH, Chong MS *et al.*: Study of gelatine-containing artificial skin V: fabrication of gelatine scaffolds using a salt-leaching method. *Biomaterials* 26(14), 1961–1968 (2005).
61. Mathieu LM, Mueller TL, Bourban P-E *et al.*: Architecture and properties of anisotropic polymer composite scaffolds for bone tissue engineering. *Biomaterials* 27(6), 905–916 (2006).
62. Zong X, Bien H, Chung C-Y *et al.*: Electrospun fine-textured scaffolds for heart tissue constructs. *Biomaterials* 26(26), 5530–5338 (2005).
63. Xu CY, Inai R, Kotaki M *et al.*: Aligned biodegradable nanofibrous structure: a potential scaffold for blood vessel engineering. *Biomaterials* 25(5), 877–886 (2004).
64. Riboldi SA, Sampaolesi M, Neuenschwander P *et al.*: Electrospun degradable polyesterurethane membranes: potential scaffolds for skeletal muscle tissue engineering. *Biomaterials* 26(22), 4606–4615 (2005).
65. Yang F, Murugan R, Wang S *et al.*: Electrospinning of nano/microscale poly(L-lactic acid) aligned fibers and their potential in neural tissue engineering. *Biomaterials* 26(15), 2603–2610 (2005).
66. Chen VJ, Smith LA, Ma PX: Bone regeneration on computer-designed nano-fibrous scaffolds. *Biomaterials* 27(21), 3973–3979 (2006).
67. Bryant SJ, Anseth KS: The effects of scaffold thickness on tissue engineered cartilage in photocrosslinked poly(ethylene oxide) hydrogels. *Biomaterials* 22(6), 619–626 (2001).
68. Boland ED, Wnek GE, Simpson DG *et al.*: Tailoring tissue engineering scaffolds using electrostatic processing techniques: a study of poly(glycolic acid) electrospinning. *Pure Appl. Chem.* A38(12), 1231–1243 (2001).
69. Boland ED, Coleman BD, Barnes CP *et al.*: Electrospinning polydioxanone for biomedical applications. *Acta Biomater.* 1(1), 115–123 (2005).
70. Kim JS, Reneker DH: *Polymer Compos.* 20, 124–131 (1999).
71. Jun HW, West JL: Endothelialization of microporous YIGSR/PEG-modified polyurethaneurea. *Tissue Eng.* 11, 1135–1140 (2005).
72. Shastri VP, Martin I, Langer R: Macroporous polymer foams by hydrocarbon templating. *Proc. Natl Acad. Sci. USA* 97(5), 1970–1975 (2000).
73. Guo HB, Miao X, Chen Y *et al.*: Charactierization of hydroxyapatite- and bioglass-316L fibre composites prepared by spark plasma sintering. *Mater. Lett.* 58(3), 304–307 (2004).
74. Hanada S, Matsumoto H, Watanabe S*: International Congress Series* 1284, 239–247 (2005).
75. Hashemi J, Chandrashekar N, Slauterbeck J: The mechanical properties of the human patellar tendon and correlated to its mass density and are independent of sex. *Clin Biomech (Bristol, Avon)* 20(6), 645–652 (2005).
76. Niebur GL, Feldstein MJ, Keaveny TM: Biaxial failure behaviour of bovine tibial trabecular bone. *J. Biomech. Eng.* 124(6), 699–705 (2002).

Websites

101. American Society of Transplant Surgeons www.asts.org/may7testimony.cfm
102. Castle Island: selective laser sintering http:home.att.net/~castleisland/sls.htm
103. MatWeb: material property data www.matweb.com

Research Article

For reprint orders, please contact: reprints@futuremedicine.com

Journal of
3D Printing in Medicine

3D segmentation of intervertebral discs: from concept to the fabrication of patient-specific scaffolds

T Oner[1,2], IF Cengiz[1,2], M Pitikakis[3], L Cesario[3], P Parascandolo[3], L Vosilla[3], G Viano[3], JM Oliveira[1,2], RL Reis[1,2] & J Silva-Correia[*,1,2]

[1]3B's Research Group – Biomaterials, Biodegradables and Biomimetics, University of Minho, Headquarters of the European Institute of Excellence on Tissue Engineering and Regenerative Medicine, Avepark – Parque de Ciência e Tecnologia, Zona Industrial da Gandra, 4805–017 Barco GMR, Portugal

[2]ICVS/3B's – PT Government Associated Laboratory, Braga, Portugal

[3]Softeco Sismat Srl, Genova, Italy

*Author for correspondence:
Tel.: +351 253 510 931
Fax: +351 253 510 909
joana.correia@dep.uminho.pt

Aim: To develop a methodology for producing patient-specific scaffolds that mimic the annulus fibrosus (AF) of the human intervertebral disc by means of combining MRI and 3D bioprinting. **Methods:** In order to obtain the AF 3D model from patient's volumetric MRI dataset, the RheumaSCORE segmentation software was used. Polycaprolactone scaffolds with three different internal architectures were fabricated by 3D bioprinting, and characterized by microcomputed tomography. **Results:** The demonstrated methodology of a geometry reconstruction pipeline enabled us to successfully obtain an accurate AF model and 3D print patient-specific scaffolds with different internal architectures. **Conclusion:** The results guide us toward patient-specific intervertebral disc tissue engineering as demonstrated by a way of manufacturing personalized scaffolds using patient's MRI data.

First draft submitted: 3 November 2016; Accepted for publication: 26 January 2017; Published online: 3 March 2017

Keywords: 3D bioprinting • intervertebral disc • MRI segmentation • patient-specific approach • rapid prototyping • reverse engineering • tissue engineering

The intervertebral disc (IVD) is a fibrocartilaginous tissue composed of a gelatinous nucleus pulposus (NP) surrounded by the cartilaginous endplates (CEP) on the upper and lower surfaces, and the annulus fibrosus (AF) laterally. The discs are the pivot point of the spine, allowing different direction movements, such as bending, rotating and twisting [1]. The primary functions of IVD are to absorb and distribute unbalanced forces through the ligaments and muscles, and to transmit spine loads that can occur as a result of motions between the vertebral bodies [2,3]. However, the IVD cannot fulfill its normal functions in pathologic conditions such as the loss of disc height (first stage of disc degeneration), endplate-driven or annulus-driven degeneration and disc herniation [4,5], and due to other reasons like physical fitness, bone mass index and smoking [6].

The current treatments mainly include the use of drugs to address the symptoms such as pain and the surgical treatments (i.e., discectomy, spinal fusion, artificial IVD replacement and the use of allogeneic or autogeneic tissues). They neither relieve pain permanently nor regenerate the tissue. Given the reported reherniation, promoted degeneration in adjacent IVDs and the changed biomechanics of the spine after the surgical treatments, it is correct to say that the clinical need has not yet been completely met [7–10]; there is a need for regenerative strategies. Tissue engineering (TE) advanced treatment strategies have promised the restoration of NP [11–15] or AF [16–19] and total disc replacement [19–21]. In simple words, in the desired TE scenario, new tissue formation occurs by extracellular matrix synthesis of implanted cells, while the biodegradable scaffold that carries and hosts the cells degrades over time. Current TE strategies consider that constructs need to have other properties besides mimicking the extracellular matrix (ECM) of the tissues to

Future Medicine part of fsg

be regenerated. The importance of developing patient-specific scaffolds is gaining a new impetus [22,23]. The need for having patient-specific IVD scaffolds is evident, given the fact that the size and shape of IVDs vary from patient to patient, and within a patient they vary within the position in the spine [1,24].

Herein, we demonstrate a step-by-step methodology to produce patient-specific scaffolds starting from the patient's MRI data. Moreover, the 3D model obtained by segmentation can also be used for the preparation and elaboration of 3D surgery planning and the assessment of its difficulties by simulating the operation before the surgical procedure [23,25].

3D reconstructions of anatomical structures are indispensable for medical diagnosis, visualization as well as 3D printing of patient-specific implants [22,26,27]. The process of 3D reconstruction of all the relevant tissues is based on the segmentation of medical imaging data. Existing image segmentation methods vary from manual slice-by-slice segmentation to fully automatic ones [28]. Attempts to fully automate the segmentation procedure are often unreliable or targeted on a limited set of specific tissues. On the other hand, interactive segmentation approaches can combine the efficiency, accuracy and repeatability of automatic methods with human expertise and quality assurance. RheumaSCORE [29], developed by Softeco Sismat S.r.l. [30], is a computer-aided diagnosis software tool that supports and assists the user in the diagnosis and the management of chronic diseases, such as rheumatoid arthritis. One of the features is that RheumaSCORE supports an interactive and real-time segmentation tool, based on a variation of the level-set algorithm for the segmentation and morphological identification of the tissues [22,31]. Other free or open source tools that can provide similar image segmentation functionality with RheumaSCORE include ITK-SNAP [32], 3D Slicer [33], GIST [34] and Analyze [35].

The level-set method [36] was employed in our previous work [22]. The level-set approach is a versatile method for the computation and analysis of the motion of an interface Γ, in two or three dimensions. It is based on the representation of a contour as the zero level set of a higher dimensional function, and formulation of the movement of the contour as the evolution of the level-set function. It is aimed to compute and analyze the subsequent motion of Γ under a velocity field $\vec{u}$. This velocity can depend on time, position, the geometry of the interface and/or external physics. The interface is captured as the zero level set of a smooth function $\varphi(x,t)$. The evolving contour/surface can be extracted from the zero level set $\Gamma(x,t) = [(x,t)|\ \varphi(x,t) = 0]$ with $\varphi:R^n \rightarrow R$. The motion function $Y(x,t)$ consists of a combination of two parts:

$$\frac{\partial \phi}{\partial t} = |\nabla \phi| \left[\alpha D(x) + (1-\alpha) \nabla \cdot \frac{\nabla \phi}{|\nabla \phi|} \right]$$

where D is a data part that forces the model toward desirable features in the input data; the part $\nabla\cdot(\nabla\varphi/|\nabla\varphi|)$ is the mean curvature of the surface, which forces the surface to have a smaller area; and $\alpha\varepsilon[0,1]$ is a free parameter that controls the degree of smoothness in the solution. There are several variants and extensions of the level-set method in the literature. One of them is the geodesic level-set method [37], which is used in the software. The distinctive characteristics of this method are that it focuses on a sparse field solver approach, and the speed function D (which acts as the principal 'force' that drives the segmentation) is the result of the combination of two terms: $D_{intensity}$ and D_{fuzzy}. The term $D_{intensity}$ is based on the input grayscale value of the voxel x, while the term D_{fuzzy} describes the affinity between contiguous voxels.

The present study is a part of the patient-specific IVD TE strategy that we envision, as depicted in Figure 1, that is, we aim to develop a standard methodology using MRI and computer-aided design combined with 3D printing for the fabrication of patient-specific IVD scaffolds from polycaprolactone (PCL) with different internal architectures. The PCL scaffolds were characterized by microcomputed tomography (μ-CT) to evaluate the effects of the internal architecture on the microstructure.

Materials & methods

MRI segmentation & 3D model reconstruction of the human IVD tissue

A 47-year-old male patient underwent an MRI scan in head-first supine position with the use of a 3.0-T scanner (Siemens MAGNETOM Spectra, Munich, Germany) using spin echo T2-weighted sequence. A Digital Imaging and Communication in Medicine (DICOM) dataset with a high spatial resolution was obtained, and the acquisition plane was sagittal. The DICOM dataset had 80 slices with a voxel size of 0.9 × 0.9 × 0.9 mm^3 and a slice thickness of 0.9 mm, with an echo time of 145 ms, repetition time of 1400 ms and an echo train length of 64.

The geometry reconstruction pipeline for generating the 3D IVD model consists of three main steps:

- Image segmentation – a proprietary software application called RheumaSCORE (v 0.1.16; Softeco Sismat S.r.l., Genova, Italy) was used for the segmentation of the MRI images. Exterior boundaries separate structures of interest and background, while interior boundaries separate anatomical areas which have different features, in other words, the

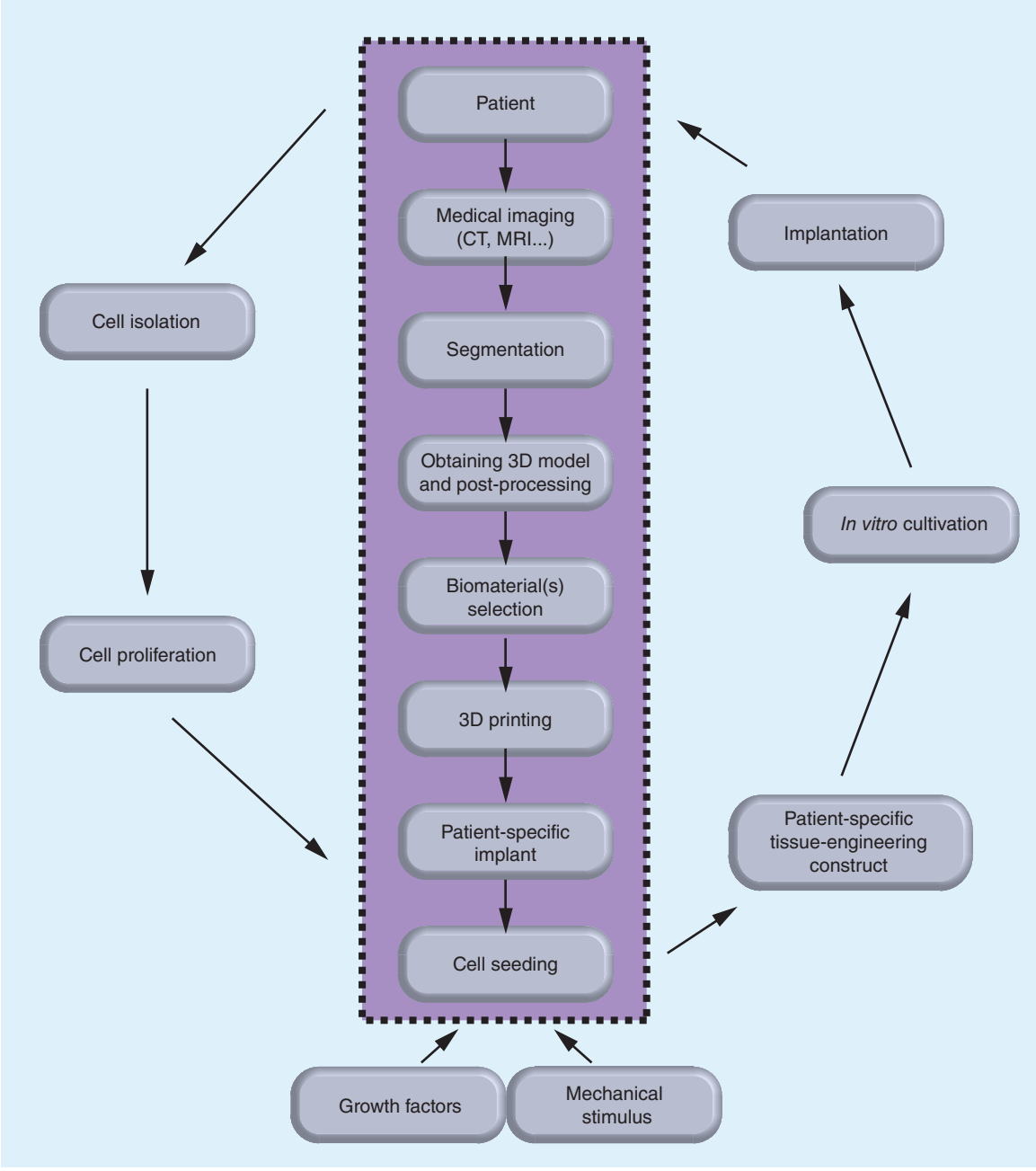

Figure 1. Representation of the envisioned patient-specific intervertebral disc tissue engineering strategy with the highlighted role of the present study in the center. The data obtained from medical imaging of the patient's intervertebral disc (IVD) are segmented and processed into a 3D model to be used in 3D printing the selected biomaterial(s) of a patient-specific IVD implant. Different types of biomaterials can be used for reproducing the annulus fibrosus and nucleus pulposus. The autologous cells are isolated from the patient, proliferated *in vitro* and introduced into patient-specific scaffold in the presence of growth factors and mechanical stimulus. The tissue engineered patient-specific construct cultured *in vitro* can be then implanted into the patient.

contact areas between the different tissues. The segmentation process is performed with an operator integration to benefit from the use of landmarks for the detection of exterior/interior borders of the contouring areas to separate CEP and AF.

- Manual corrections on the segmented images – some manual refinements were needed to improve the accuracy of the segmented images. The user interface of the tool allows manual error corrections after segmentation or during segmentation using the draw/erase mode.

- 3D reconstruction – from a given 3D scalar field of voxels, all boundary surfaces are to be computed. The 3D model reconstruction was obtained from the segmented images, and the 3D model was converted into a stereolithography format using the software, which includes this 3D model generation and conversion to stereolithography feature.

Fabrication of patient-specific IVD scaffolds

The 3D model of the IVD was isotropically resized to half size to be practical, and sliced into 0.167-mm-thick layers with the software provided by EnvisionTec GmbH (Germany). Using a fourth-generation 3D Bioplotter (EnvisionTec GmbH, Dearborn, Michigan, USA), three patient-specific IVD scaffolds were printed with three different internal architectures resulting from a layer-wise alternating strand directions either as 0°/90° (architecture A), 0°/60°/120° (architecture B) or 0°/45°/90°/135° (architecture C). In each layer, the strands were parallel to each other and 1 mm apart from each other. For printing the scaffolds, PCL (average M_n = 45,000) purchased from Sigma-Aldrich (MO, USA) was melted at 110°C in the cartridge of the 3D Bioplotter and extruded as strands through a 22G heated metal needle, at a speed of 5 mm/s and under the pressure of 5 bar.

μ-CT analysis

Three samples of each of the three architectures were scanned with a high-resolution desktop x-ray μ-CT system (SkyScan 1272; Bruker MicroCT, Kontich, Belgium) for the 3D morphometric analysis. The x-ray source voltage and current were set at 50 kV and 200 μA, respectively. About 800 projections with 10 μm of isotropic pixel size were acquired over a rotation range of 360° with a rotation step of 0.45°. The 2D cross-sectional images were reconstructed from the x-ray projections. On each 2D images, a grayscale threshold of 32–255 was applied, and a region of interest was defined to obtain a volume of interest dataset which was used for the 3D morphometric analysis performed by using the CT Analyser software (version 1.15.4.0) supplied by Bruker MicroCT.

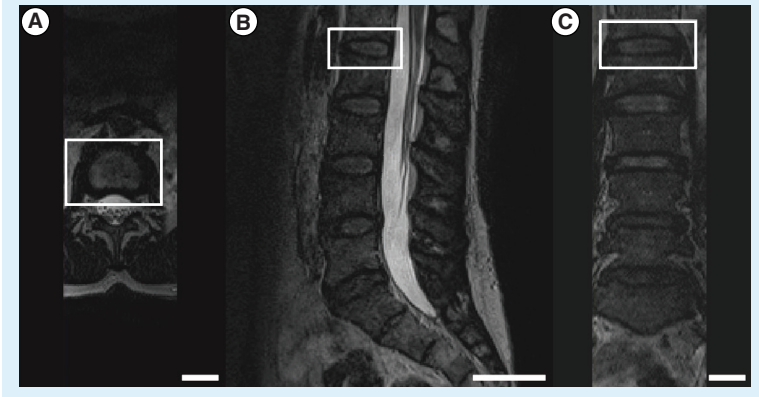

Figure 2. MRI images of the patient. Images taken from the **(A)** axial, **(B)** sagittal and **(C)** coronal planes. The L1–L2 intervertebral disc was indicated by the white rectangle (scale bars: 4 cm).

Statistical analysis

Statistical analysis was performed using SPSS® (IBM® SPSS® Statistics version 23.0; IBM, USA). One-way analysis of variance (ANOVA) tests were used to determine the statistically significant differences between the three different architectures in each structural property (i.e., mean pore size, porosity and interconnectivity). The level of significance used was set at $p < 0.05$ for a 95% CI.

Results & discussion

MRI segmentation & 3D human IVD model reconstruction

The DICOM dataset having 80 3D T2-weighted MRI images with a voxel size of 0.9 × 0.9 × 0.9 mm^3 was obtained for the segmentation of the L1–L2 IVD of the patient. Figure 2 shows the MRI images of the patient from different planes. In our work, we utilized the RheumaSCORE software which uses a variation of the level-set algorithm. CEP and AF have similar intensity on the 2D images; therefore, the landmarks were identified manually inside the interest region of the 2D images for the detection of exterior/interior borders of the contouring areas to distinguish CEP and AF. Also, with the use of the presegmentation tool of RheumaSCORE, that is, grayscale thresholding function, it was possible to segment the AF without the NP component of the IVD. From the final image segmentation, a 3D surface model was reconstructed with RheumaSCORE (Figure 3). A requirement for having high-quality 3D models is to have volumetric images with identical resolution in all dimensions, that is, isotropic. The DICOM images of the patient were almost isotropic and with high spatial resolution. For a precise segmentation, besides having a high spatial resolution, it is also necessary to obtain the accurate geometric structure of the IVD. Based on our work, an MRI with a smaller voxel size was possible to achieve. Nevertheless, a smaller voxel size may cause a high noise that dramatically affects the segmentation quality, and the final outcome can be worse. The high noise results from long acquisition time and involuntary movement of the spine of the patient during the MRI acquisition process.

In this study, T2-weighted MRI was used as medical image visualization and a semiautomatic

segmentation was performed for segmentation of the disc, as an alternative to manual and automatic segmentation. Since manual segmentation is a completely operator-dependent and time-consuming process, the manually drawing of the region of interest requires proper skills and adequate software tools with sophisticated graphical user interface [38]. On the other hand, semiautomatic segmentation has been proposed to minimize supervised operator needs of manual segmentation as well as to allow error correction during the segmentation process, unlike automatic segmentation.

Although we have used the acquired 3D IVD model to produce scaffold, the proposed model can be utilized for several other objectives including, but not limited to, finite element modeling [39]. In addition, the 3D models of the IVD and spine may be preferred over the 2D images by the surgeon for the presurgery planning.

In the last decade, level-set methods which have emerged for the segmentation of images [40], are based on a calculus of piecewise constant variational equations. Moreover, the method can represent contours with complex topology and allow any topological changes naturally. Experiments related to the segmentation of the IVDs were performed using the level-set algorithm, and the segmentation method was determined as a semiautomatic mode which uses a combination of supervised active contour segmentation and postprocessing carried out manually in the following slices. In MRI, hard and soft tissues can be roughly discriminated by characteristic scalar values, in other words, grayscale. Thus, they can be quickly computed as isosurfaces, that is, surfaces passing through voxels of the same scalar value. Typically, anatomical structures are in complex shape, and their curved boundary surfaces are essential to preserve. These boundary surfaces are represented by a set of triangles that are convenient to render using graphics hardware. However, CEP and AF have similar scalar values. Therefore, there is a need for some amount of user interaction. To address this issue, we are currently working to develop a methodology to fully automate the IVD segmentation process; this procedure will allow enhancing the accuracy and reproducibility of the segmentation while minimizing workload, user interaction and extensive postprocessing after the segmentation.

3D fabrication of patient-specific IVD scaffolds

The 3D patient-specific IVD model (Figure 4) was obtained by the segmentation of the MRI. The dataset was isotropically resized to half size and sliced into 25 layers possessing a thickness of 0.167 mm each (Figure 5A & B). Three distinct internal architectures were developed as shown in Figure 5C–E. The architectures of scaffolds A–C are composed of alternating layers of 0°/90°, 0°/60°/120° and 0°/45°/90°/135° strands, respectively. Figure 6 shows the 3D-printed patient-specific IVD scaffolds with different architectures. Herein, a methodology from MRI acquisition to the 3D-printed IVD scaffolds has been demonstrated to be the critical part of the envisioned patient-specific IVD TE strategy. PCL was selected as the biomaterial for the 3D printing because it is a biomaterial that gathers appropriate properties for rapid prototyping. Once the patient-specific IVD model is obtained, it is possible to tailor the scaffold architecture, as such three basic architectures were studied; and a higher number of different and more complex architectures can be designed.

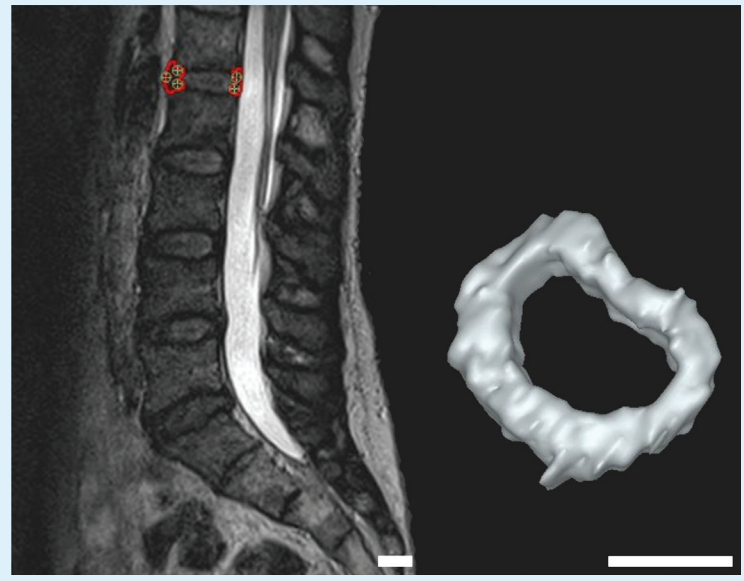

Figure 3. The segmentation process. Left: L1–L2 intervertebral disc of the patient. Right: the 3D model of the intervertebral disc after completing the segmentation (scale bars: 2 cm).

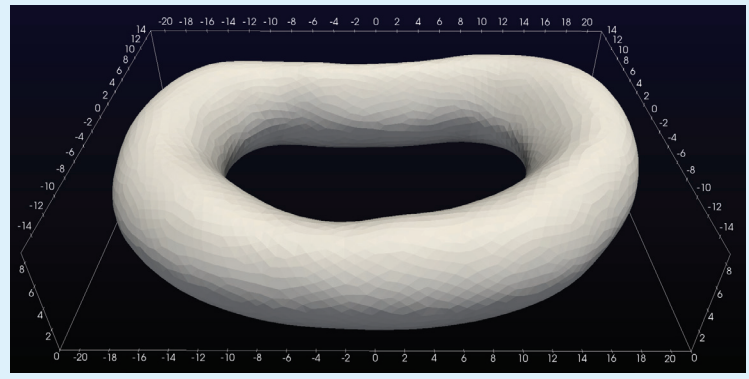

Figure 4. The final smoothed 3D model of the L1–L2 intervertebral disc of the patient. The numbers correspond to millimeter.

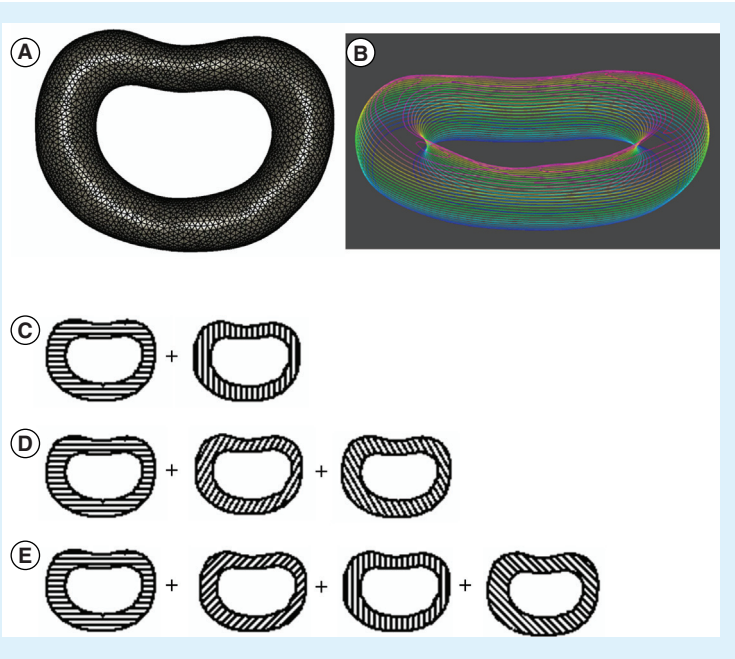

Figure 5. Patient-specific 3D intervertebral disc model, its layers, and the layer-wise alternating strand directions. (A) The wireframe 3D model of the intervertebral disc (IVD) of the patient; **(B)** the layers of the 3D IVD model after slicing of the 3D model into layers with colors changing from red to blue indicating the top and the bottom layer, respectively; the illustration of the alternating layers in the three architectures: architectures A–C with **(C)** 0°/90°, **(D)** 0°/60°/120° and **(E)** 0°/45°/90°/135° strand structures, respectively.

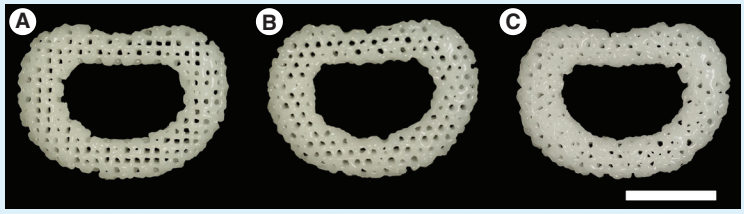

Figure 6. Photographs of the 3D printed intervertebral disc scaffolds with three different internal architectures. (A) Architecture A (0°/90° strand structure). **(B)** Architecture B (0°/60°/120° strand structure). **(C)** Architecture C (0°/45°/90°/135° strand structure) (scale bars: 1 cm).

We have demonstrated a step-by-step methodology to produce patient-specific scaffolds starting from the patient's MRI data. Moreover, the 3D model obtained through segmentation can also be used for the preparation and elaboration of 3D surgery planning and the assessment of its difficulties by simulating the operation before the surgical procedure [23,25]. With the aim of moving further with the knowledge arising from the present studies, the methodology herein demonstrated is currently being investigated for obtaining complex IVD TE implants by means of combining bio-inks (e.g., silk fibroin and methacrylated gellan gum hydrogels) and stem cells.

μ-CT analysis of the 3D-printed scaffolds

The structural and morphometric features of the 3D-fabricated samples with the three different architectures were analyzed by μ-CT. The 2D and 3D images are shown in Figure 7. The μ-CT analysis revealed that the three architectures had similar porosity and interconnectivity, but having different mean pore sizes as summarized in Table 1, and the pore size distributions are shown in Figure 8. ANOVA tests were carried out to investigate if there are any statistically significant differences in each structural feature between the different architectures. The mean pore size was statistically significantly different for each architecture: $F(2, 6) = 218.7$, $p < 0.0005$, $\Omega^2 = 0.98$ and partial $\eta^2 = 0.99$. Based on the Cohen's effect size benchmarks [41,42], the η^2 values of 0.01, 0.06 and 0.14 correspond to small, medium and large effect size classes, respectively. The pairwise differences were investigated with the Tukey's posthoc analysis. There was a statistically significant difference of 165.1 (95% CI: 40.1, 190.1) between architectures A and B (mean [M] = 555.3, standard error [SE] = 9.0) and a difference of 45.5 (95% CI: 20.5, 70.5) in mean pore size between architecture A (M = 600.8, SE = 3.8) and architecture C (M = 435.7, SE = 2.2). When architectures B and C were compared, there was a statistically significant difference of 119.6 (95% CI: 94,6, 144.6; $p < 0.0005$). The architectures were not statistically significantly different regarding the porosity $F(2, 6) = 0.892$; $p = 0.458$, and interconnectivity. $F(2, 6) = 1.034$; $p = 0.411$.

The null hypothesis in the ANOVA tests was that the means of the samples with architectures A–C are equal for a structural property; and the alternative hypothesis was that at least the mean of one architecture is different. For the mean pore size, the null hypothesis was rejected, and the alternative hypothesis was accepted since the means of the groups were statistically significantly different; and the null hypothesis cannot be rejected for porosity and interconnectivity.

The entire data were checked for the presence of outliers, normal distribution and homogeneity of variances to ensure statistically valid results by confirming the assumptions that underlie the ANOVA tests were met. There were no outliers as assessed by inspection of a box plot for values of >1.5 box lengths from the edge of the box. The data were normally distributed as determined by Shapiro–Wilk's test ($p > 0.05$). There was homogeneity of variances confirmed by Levene's test for equality of variances ($p = 0.093$ for mean pore size, $p = 0.716$ for porosity, $p = 0.241$ for interconnectivity).

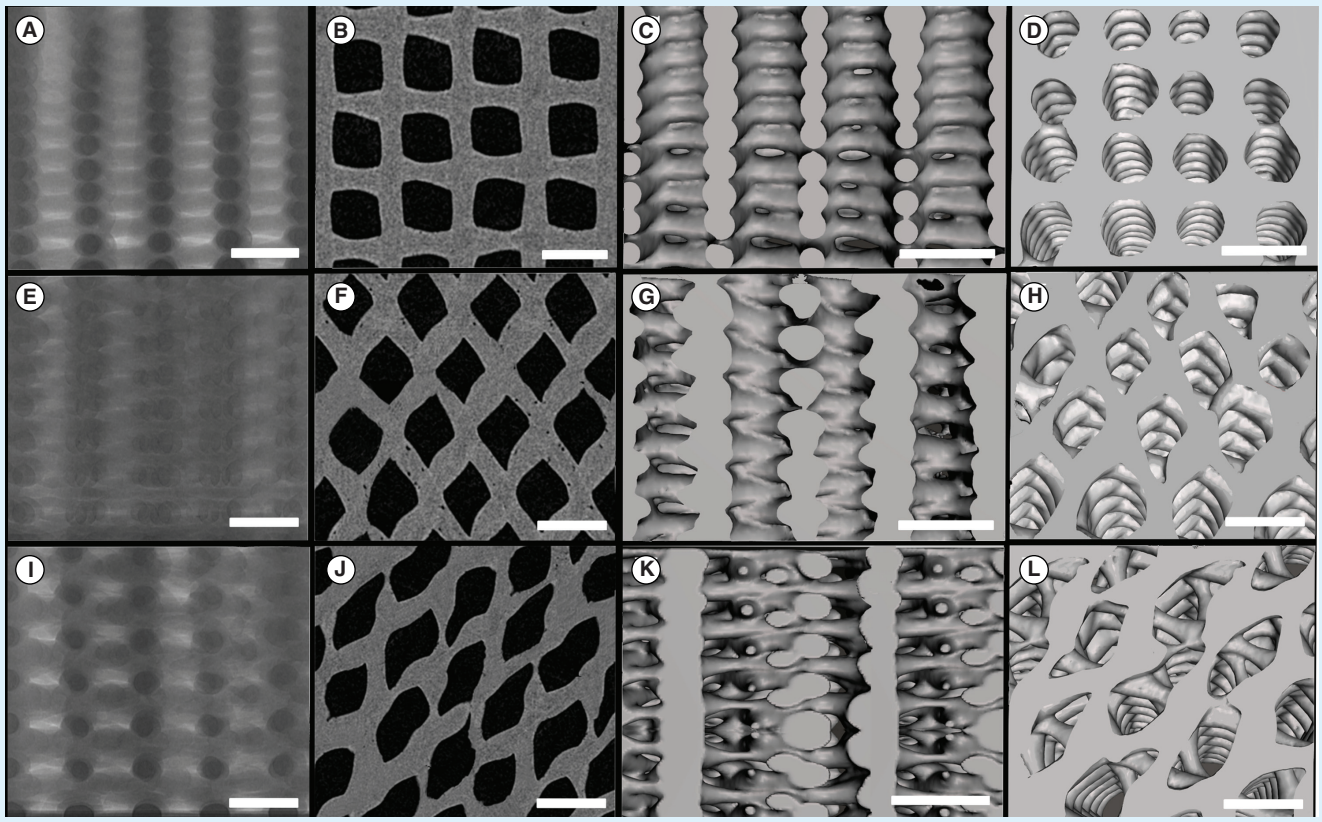

Figure 7. The μ-CT images of the 3D printed samples with the three different internal architectures. (Top row: A–D) A (0°/90° strand structure), **(middle row: E–H)**, B (0°/60°/120° strand structure) and **(bottom row: I–L)** C (0°/45°/90°/135° strand structure): the x-ray images **(A, E and I)**, the 2D reconstructed microcomputed tomography images **(B, F and J)**, the 3D reconstructed images showing the structures from side **(C, G and K)** and top **(D, H and L)** (scale bars: 1 mm).

The size of the pores is one of the important features of a scaffold since it influences the cell attachment, growth and matrix production [43–46]. In the present study, the architecture of PCL scaffolds B and C, which possess micropores, is more adequate for cell culturing as compared with PCL scaffold A (Figure 8). Rebelo *et al.* [47] reviewed the cellular morphometry and characteristics of IVD. It was reported that the fibroblasts have the diameter of 1–20 μm and the chondrocytes have the size of around 10–30 μm. The convenience of diffusion and migration of cells is related to relatively larger sized pores, while cell adhesion is related to relatively smaller sized pores since the relative surface area is larger [45]. Matsiko *et al.* [48] demonstrated that the microarchitecture of the scaffold has a role in differentiation and matrix synthesis of cells. Among the scaffolds they studies, they reported that the scaffolds with the mean pore size

Table 1. The structural and morphometric properties of the scaffolds with the three distinct internal architectures of A (0°/90° strand structure), B (0°/60°/120° strand structure) and C (0°/45°/90°/135° strand structure).

Internal architecture	A	B	C
Porosity (%) M(SE)	45.8 (0.9)	45.8(1.3)	44.1 (1.0)
Mean pore size (μm) M(SE)	600.8 (3.8)	555.3 (9.0)	435.7 (2.2)
Interconnectivity (%) M(SE)	99.2 (0.1)	99.0 (0.1)	99.1 (0.1)

M: Mean; SE: Standard error.

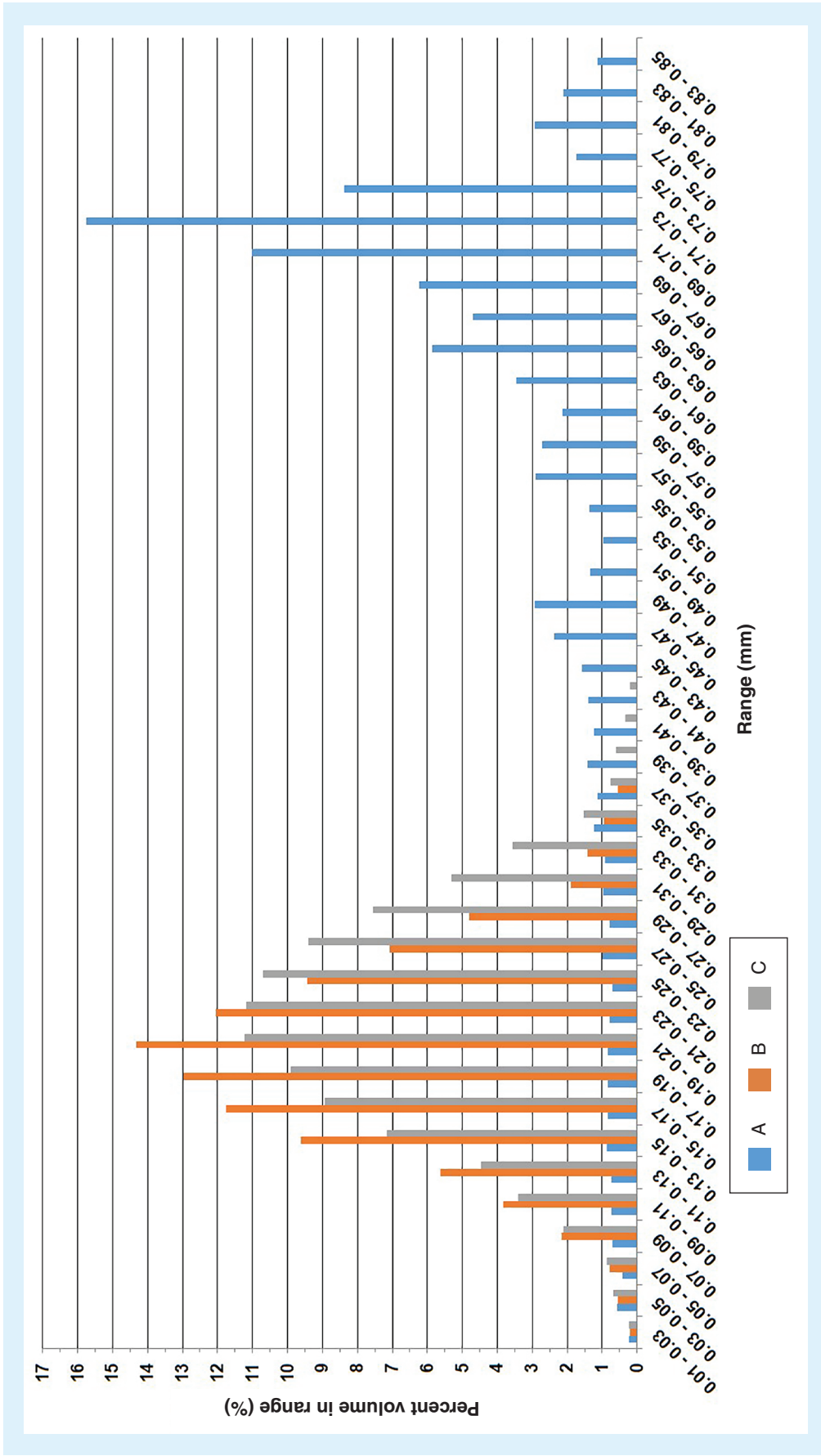

Figure 8. The pore size distribution of the samples with the three distinct internal architectures. (A) (0°/90° strand structure), **(B)** (0°/60°/120° strand structure) and **(C)** (0°/45°/90°/135° strand structure).

of 300 µm provided higher cell growth, like matrix production compared with the scaffolds with the smaller mean pore size that are 94 and 130 µm [48]. Zhang *et al.* [49] 3D-printed PCL scaffolds with three different mean pore sizes, 215, 320 and 515 µm. The authors reported that the scaffolds with the mean pore size of 215 µm had relatively higher cell growth and matrix synthesis *in vitro*, and better performance compared with others *in vivo* [49].

In brief, future studies should further investigate the effect of the scaffold microstructure on the biological and biomechanical performance in a broader manner, that is, considering not only the mean pore size but also the mean porosity and mean wall thickness of the scaffolds.

Conclusion

This study showed a semiautomatic methodology of a geometry reconstruction pipeline from volumetric medical image data to 3D meshes of patient-specific IVD model. The obtained 3D model was 3D printed into scaffolds with different internal architectures. The present work steers us toward the patient-specific IVD TE concept as demonstrated in a way of manufacturing patient-specific scaffolds using the 3D model obtained from the patient's MRI. Furthermore, the obtained patient-specific model could aid in the improvement of clinical and surgical planning before treatment.

Financial & competing interests disclosure

The authors would like to acknowledge the financial support provided by the Portuguese Foundation for Science and Technology (FCT) through the project EPIDisc (UTAP-EXPL/BBB-ECT/0050/2014), funded in the Framework of the 'International Collaboratory for Emerging Technologies, CoLab', UT AustinlPortugal Program. FCT is also acknowledged for the PhD scholarship attributed to IF Cengiz (SFRH/BD/99555/2014) and the financial support provided to J Silva-Correia (SFRH/BPD/100590/2014 and IF/00115/2015). JM Oliveira also thanks the FCT for the funds provided under the program Investigador FCT (IF/00423/2012 and IF/01285/2015). The authors have no other relevant affiliations or financial involvement with any organization or entity with a financial interest in or financial conflict with the subject matter or materials discussed in the manuscript apart from those disclosed.

No writing assistance was utilized in the production of this manuscript.

Ethical conduct of research

The authors state that they have obtained appropriate institutional review board approval or have followed the principles outlined in the Declaration of Helsinki for all human or animal experimental investigations. In addition, for investigations involving human subjects, informed consent has been obtained from the participants involved.

Executive summary

- The clinical need has not been yet completely met to treat intervertebral disc (IVD) problems, and there is a need for regenerative tissue engineering (TE) strategies.
- Scaffolds hold a critical role in IVD TE.
- Given the fact that IVDs differ in size and shape, being patient-specific holds a great importance.
- To show how to produce patient-specific IVD scaffolds/implants, we presented a methodology for producing such 3D-printed scaffolds from human MRI using a semiautomatic 3D segmentation.
- Scaffolds with different internal architectures were produced, and their effect on the microstructure was compared with get preindications on their biological performances with cells.
- Medical imaging combined with the 3D-printing technology enables us to proceed directly to produce patient-specific implants from the chosen biomaterial/s.
- The results bring us a step closer to the development of patient-specific IVD TE scaffold, and the translation into daily clinical approaches is envisioned with future studies.

References

Papers of special note have been highlighted as:
• of interest; •• of considerable interest

1 Shankar H, Scarlett JA, Abram SE. Anatomy and pathophysiology of intervertebral disc disease. *Tech. Reg. Anesth. Pain Manag.* 13(2), 67–75 (2009).

2 Silva-Correia J, Correia SI, Oliveira JM, Reis RL. Tissue engineering strategies applied in the regeneration of the human intervertebral disk. *Biotechnol. Adv.* 31(8), 1514–1531 (2013).

• **Provides the reader a very good overview of the intervertebral disc (IVD) tissue engineering.**

3 Nerurkar NL, Elliott DM, Mauck RL. Mechanical design criteria for intervertebral disc tissue engineering. *J. Biomech.* 43(6), 1017–1030 (2010).

4 Adams MA, Roughley PJ. What is intervertebral disc degeneration, and what causes it? *Spine* 31(18), 2151–2161 (2006).

• **Provides the reader a very good overview of the IVD anatomy, physiology and degeneration.**

5 Adams MA, Dolan P. Intervertebral disc degeneration: evidence for two distinct phenotypes. *J. Anat.* 221(6), 497–506 (2012).

6 Depalma MJ, Ketchum JM, Saullo TR. Multivariable analyses of the relationships between age, gender, and body mass index and the source of chronic low back pain. *Pain Med.* 13(4), 498–506 (2012).

7 Lebow RL, Adogwa O, Parker SL, Sharma A, Cheng J, Mcgirt MJ. Asymptomatic same-site recurrent disc herniation after lumbar discectomy: results of a prospective longitudinal study with 2-year serial imaging. *Spine* 36(25), 2147–2151 (2011).

8 Cowan JA Jr, Dimick JB, Wainess R, Upchurch GR Jr, Chandler WF, La Marca F. Changes in utilization of spinal fusion in the United States. *Neurosurgery* 59(1), 15–20 (2006).

9 Whatley BR, Wen X. Intervertebral disc (IVD): structure, degeneration, repair and regeneration. *Mater. Sci. Eng. C* 32(2), 61–77 (2012).

• **Provides the reader a very good overview of the IVD degeneration and repair.**

10 Barrey C, Perrin G, Champain S. Pedicle-screw-based dynamic systems and degenerative lumbar diseases: biomechanical and clinical experiences of dynamic fusion with isobar TTL. *ISRN Orthop.* 2013, 183702 (2013).

11 Silva-Correia J, Oliveira JM, Caridade SG *et al.* Gellan gum-based hydrogels for intervertebral disc tissue-engineering applications. *J. Tissue Eng. Regen. Med.* 5(6), e97–107 (2011).

12 Silva-Correia J, Miranda-Gonçalves V, Salgado AJ *et al.* Angiogenic potential of gellan-gum-based hydrogels for application in nucleus pulposus regeneration: *in vivo* study. *Tissue Eng. Part A* 18(11–12), 1203–1212 (2012).

13 Pereira D, Silva Correia J, Oliveira JM, Reis R. Hydrogels in acellular and cellular strategies for intervertebral disc regeneration. *J. Tissue Eng. Regen. Med.* 7(2), 85–98 (2013).

•• **Provides the reader a very good overview of the hydrogels for IVD regeneration.**

14 Reitmaier S, Kreja L, Gruchenberg K *et al. In vivo* biofunctional evaluation of hydrogels for disc regeneration. *Eur. Spine J.* 23(1), 19–26 (2014).

15 Silva-Correia J, Gloria A, Oliveira MB *et al.* Rheological and mechanical properties of acellular and cell laden methacrylated gellan gum hydrogels. *J. Biomed. Mater. Res. A* 101(12), 3438–3446 (2013).

16 Mizuno H, Roy AK, Vacanti CA, Kojima K, Ueda M, Bonassar LJ. Tissue-engineered composites of anulus fibrosus and nucleus pulposus for intervertebral disc replacement. *Spine* 29(12), 1290–1297 (2004).

17 Saad L, Spector M. Effects of collagen type on the behavior of adult canine annulus fibrosus cells in collagen–glycosaminoglycan scaffolds. *J. Biomed. Mater. Res. A* 71(2), 233–241 (2004).

18 Shao X, Hunter CJ. Developing an alginate/chitosan hybrid fiber scaffold for annulus fibrosus cells. *J. Biomed. Mater. Res. A* 82(3), 701–710 (2007).

19 Van Uden S, Silva-Correia J, Correlo V, Oliveira J, Reis R. Custom-tailored tissue engineered polycaprolactone scaffolds for total disc replacement. *Biofabrication* 7(1), 015008 (2015).

20 Park SH, Gil ES, Mandal BB *et al.* Annulus fibrosus tissue engineering using lamellar silk scaffolds. *J. Tissue Eng. Regen. Med.* 6(S3), S24–S33 (2012).

21 Park SH, Gil ES, Cho H *et al.* Intervertebral disk tissue engineering using biphasic silk composite scaffolds. *Tissue Eng. Part A* 18(5–6), 447–458 (2011).

22 Cengiz IF, Pitikakis M, Cesario L *et al.* Building the basis for patient-specific meniscal scaffolds: from human knee MRI to fabrication of 3D printed scaffolds. *Bioprinting* 1–2, 1–10 (2016).

•• **Successfully produced patient-specific implants from MRI data.**

23 Radenkovic D, Solouk A, Seifalian A. Personalized development of human organs using 3D printing technology. *Med. Hypotheses* 87, 30–33 (2016).

24 Lertudomphonwanit T, Keorochana G, Kraiwattanapong C, Chanplakorn P, Leelapattana P, Wajanavisit W. Anatomic considerations of intervertebral disc perspective in lumbar posterolateral approach via Kambin's triangle: cadaveric study. *Asian Spine J.* 10(5), 821–827 (2016).

25 Cevidanes LH, Tucker S, Styner M *et al.* Three-dimensional surgical simulation. *Am. J. Orthod. Dentofacial Orthop.* 138(3), 361–371 (2010).

26 Gander T, Essig H, Metzler P *et al.* Patient specific implants (PSI) in reconstruction of orbital floor and wall fractures. *J. Craniomaxillofac. Surg.* 43(1), 126–130 (2015).

27 Kozakiewicz M, Elgalal M, Walkowiak B, Stefanczyk L. Technical concept of patient-specific, ultrahigh molecular weight polyethylene orbital wall implant. *J. Craniomaxillofac. Surg.* 41(4), 282–290 (2013).

28 Pham DL, Xu C, Prince JL. Current methods in medical image segmentation. *Annu. Rev. Biomed. Eng.* 2(1), 315–337 (2000).

29 RheumaSCORE. www.research.softeco.it/rheumascore.aspx (2016).

30 Softeco Sismat S.r.l. www.softeco.it (2016).

31 Parascandolo P, Cesario L, Vosilla L, Viano G. Computer aided diagnosis: state-of-the-art and application to musculoskeletal diseases. In: *3D Multiscale Physiological Human*, Magnenat-Thalmann N, Ratib O, Choi HF (Eds). Springer-Verlag, London, UK, 277–296 (2014).

32 Yushkevich PA, Piven J, Hazlett HC *et al.* User-guided 3D active contour segmentation of anatomical structures: significantly improved efficiency and reliability. *Neuroimage* 31(3), 1116–1128 (2006).

33 3Dslicer. www.slicer.org (2016).

34 Cates JE, Lefohn AE, Whitaker RT. GIST: an interactive, GPU-based level set segmentation tool for 3D medical images. *Med. Image Anal.* 8(3), 217–231 (2004).

35 Analyze. www.analyzedirect.com (2016).

36 Parascandolo P, Cesario L, Vosilla L, Pitikakis M, Viano G. Smart Brush: a real time segmentation tool for 3D medical images. Presented at: *8th International Symposium on Image and Signal Processing and Analysis (ISPA)*, Trieste, Italy, September 4–6, 2013.

• **Successfully showed 3D segmentation on medical images.**

37 Caselles V, Kimmel R, Sapiro G. Geodesic active

contours. Presented at: *Proceedings of the Fifth International Conference on Computer Vision*. Cambridge, MA, USA, June 20–23, 1995.

38 Wong KP. Medical image segmentation: methods and applications in functional imaging. In: *Handbook of Biomedical Image Analysis*. Suri JS, Wilson DL, Laxminarayan S (Eds). Springer-Verlag, London, UK, 111–182 (2005).

39 Cortez S, Claro JCP, Alves J. 3D reconstruction of a spinal motion segment from 2D medical images: objective quantification of the geometric accuracy of the FE mesh generation procedure. Presented at: *IEEE 3rd Portuguese Meeting in Bioengineering (ENBENG)*. Braga, Portugal, February 20–23, 2013.

40 Kimmel R. *Numerical Geometry of Images: Theory, Algorithms, and Applications*. Springer-Verlag, NY, USA (2012).

41 Cohen J. *Statistical Power Analysis for the Behavioral Sciences* (2nd Edition). Lawrence Erlbaum Associates, NJ, USA (1988).

42 Ellis PD. *The Essential Guide to Effect Sizes: Statistical Power, Meta-Analysis, and The Interpretation of Research Results*. Cambridge University Press, Cambridge, UK (2010).

43 Murphy CM, Duffy GP, Schindeler A, O'brien FJ. Effect of collagen–glycosaminoglycan scaffold pore size on matrix mineralization and cellular behavior in different cell types. *J. Biomed. Mater. Res. A* 104(1), 291–304 (2016).

44 Zhang Q, Lu H, Kawazoe N, Chen G. Pore size effect of collagen scaffolds on cartilage regeneration. *Acta Biomater.* 10(5), 2005–2013 (2014).

45 O'brien FJ, Harley B, Yannas IV, Gibson LJ. The effect of pore size on cell adhesion in collagen–GAG scaffolds. *Biomaterials* 26(4), 433–441 (2005).

46 Murphy CM, Haugh MG, O'brien FJ. The effect of mean pore size on cell attachment, proliferation and migration in collagen–glycosaminoglycan scaffolds for bone tissue engineering. *Biomaterials* 31(3), 461–466 (2010).

47 Rebelo MA, Alves TF, De Lima R *et al.* Scaffolds and tissue regeneration: an overview of the functional properties of selected organic tissues. *J. Biomed. Mat. Res. Part B: Applied Biomaterials*. 104 (7) 1483–1494 (2016).

48 Matsiko A, Gleeson JP, O'brien FJ. Scaffold mean pore size influences mesenchymal stem cell chondrogenic differentiation and matrix deposition. *Tissue Eng. Part A* 21(3–4), 486–497 (2014).

49 Zhang ZZ, Jiang D, Ding JX *et al.* Role of scaffold mean pore size in meniscus regeneration. *Acta Biomater.* 43, 314–326 (2016).

Review

For reprint orders, please contact: reprints@futuremedicine.com

Regenerative Medicine

Strategies for bioengineered scaffolds that support adipose stem cells in regenerative therapies

Regenerative medicine possesses the potential to ameliorate damage to tissue that results from a vast range of conditions, including traumatic injury, tumor resection and inherited tissue defects. Adult stem cells, while more limited in their potential than pluripotent stem cells, are still capable of differentiating into numerous lineages and provide feasible allogeneic and autologous treatment options for many conditions. Adipose stem cells are one of the most abundant types of stem cell in the adult human. Here, we review recent advances in the development of synthetic scaffolding systems used in concert with adipose stem cells and assess their potential use for clinical applications.

First draft submitted: 27 May 2016; Accepted for publication: 12 July 2016; Published online: 3 August 2016

Keywords: 3D scaffolds • adipose-derived stem cells • ASC • cartilaginous regeneration • osteogenic regeneration • regenerative medicine • soft-tissue regeneration • synthetic scaffold

Tracy N Clevenger[1,2,3,4], Gabriel Luna[2,5], Steven K Fisher[2,5] & Dennis O Clegg*[,1,2,3,4]

[1]Center for Stem Cell Biology & Engineering, University of California, Santa Barbara, CA, USA

[2]Neuroscience Research Institute, University of California, Santa Barbara, CA, USA

[3]Department of Molecular, Cellular & Developmental Biology, University of California, Santa Barbara, CA, USA

[4]Institute for Collaborative Biotechnologies, University of California, Santa Barbara, CA, USA

[5]Center for Bio-Image Informatics, University of California, Santa Barbara, CA, USA

*Author for correspondence: dennis.clegg@lifesci.ucsb.edu

Stem cells in regenerative medicine

Regenerative medicine is an immense field focused on the replacement, and regeneration of human cells and/or tissues to restore normal functions [1,2]. The replacement of damaged or diseased tissue with functioning healthy cells is the primary goal of this field. The use of stem cells has become fundamental to its rapid expansion and the foundation for developing therapies to treat congenital defects, traumatic injury and disease in a patient-specific manner through the use of autologous tissue [3]. Since the first documented use of the term 'regenerative medicine' and the isolation of human embryonic stem cells, efforts to develop synthetic scaffolds for use in conjunction with stem cells have increased significantly [4–6]. The use of stem cells for regenerative treatments has achieved varying degrees of success with regards to replacing missing or damaged tissue, but progressive improvements have been brought about via recent efforts in tissue engineering [7].

Indeed, a PubMed search for 'regenerative medicine' yields more than 30,000 publications since 1920 [8]. When the search is narrowed to include 'regenerative medicine and stem cells' a list of 11,770 publications is returned. Refining this search still further by using key words such as 'mesenchymal stem cells' yields only 1148 publications. Finally, using the phrase 'regenerative medicine and adipose-derived stem cell' (ASC) produces a total of 156 publications from 2005 to 2016, an indication that research involving ASCs in the field of regenerative medicine remains in its infancy.

Surgeons in the American Society of Plastic Surgeons preformed more than 5.8 million reconstructive surgeries in 2015 alone to repair defects arising from tumor resection, traumatic injury, maxillofacial abnormalities, laceration repair and scar revision [9]. However, even the most common treatments show a significant and unpredictable loss of transplanted tissue volume over time. Volume loss

Future Medicine part of fsg

is a main reason for treatment failure, and therefore a need exists for a microenvironment that produces repeatable, sustainable results over many years. To this end, a biologically inert scaffolding system that can be tailored to the needs of individual patients and presents a means for maintaining tissue volume may prove to be a significant advancement over current treatments.

Bone marrow-derived mesenchymal stem cells (BM-MSCs) are a type of adult stem cell commonly used in numerous therapies including liver failure as a result of hepatitis B [10]. BM-MSCs have been approved for use in humans since 1995, and are currently being used in 272 clinical trials according to clinicaltrials.gov. However, unlike pluripotent embryonic stem cells, MSCs are multipotent cells that possess the ability to differentiate into various cell types, including adipogenic, chondrogenic, osteogenic, muscular, cardiac and endothelial lineages [11–15]. The International Society for Cellular Therapy (ISCT) uses three criteria to define MSCs regardless of their source: first, plastic adherence in standard culture conditions; second, expression of nonspecific surface markers CD105, CD90 and CD73 and the absence of CD34, CD45, CD14 or CD11b, CD79α and HLA-DR; and third, differentiation into osteoblasts, adipocytes and chondroblasts under specific stimuli *in vitro* [16,17]. The benefits of using adult MSCs for treatments include the ability for autologous transplants and the absence of ethical controversies surrounding their use. Adipose tissue provides an alternative high-yield source of adult stem cells known as ASCs that are predominately obtained through rudimentary liposuction procedures [18,19].

ASCs share many similarities with BM-MSCs including their potential to develop into similar cell lineages and have no clear distinction between the populations in terms of surface marker or gene expression [16,20–23]. It has been suggested that ASCs can be distinguished from BM-MSCs by their expression of CD36 (F.A.T. – a protein involved in fatty acid metabolism) or CD49d (integrin α4 – a subunit of the integrin receptor for fibronectin and VCAM-1), as well as the lack of CD106 (VCAM1 – a protein involved in the adhesion of vascular cells). However, each of these proteins shows variability in expression patterns between specific ASC populations [24]. Investigations into the gene expression profiles of BM-MSCs and ASCs found that 13.2% of 384 genes examined were differentially expressed between the two populations. Although no identifying markers were specific to each population, genes more highly expressed by ASCs were mainly involved in cellular communication (*FGF9*, *IL1R2*, *CCL3* and *KDR*) while those with higher expression by BM-MSCs were involved in WNT signaling and differentiation pathways (*WNT11*, *WNT7B* and *SOX6*) [25].

ASCs are ten-times more abundant than BM-MSCs in the tissues from which they are isolated. Additionally, ASCs demonstrate a higher proliferative potential, show consistent growth rates in culture and are procured from a minimally invasive procedure by comparison [26,27]. Furthermore, ASCs are robust, capable of self-renewal, can be collected in large quantities and easily expanded in culture. These qualities identify ASCs as a promising source for use in therapeutic regenerative medicine [28–31].

Over the last 18 years, many techniques have been developed to create scaffolding materials that are compatible with stem cells as well as transplantation sites. Scaffolds generated prior to cell seeding allow for the use of reagents typically considered 'harsh,' thereby expanding the potential library of materials for therapeutic use. Topical seeding of cells has been one approach used in the development of synthetic scaffolds in regenerative medicine, but often results in a very low penetration throughout the material, leading to a heterogeneous cellular distribution within the scaffold [32]. Another tactic for the development of scaffolds as regenerative therapies is the use of decellularized extracellular matrix (ECM). These scaffolds are generated from allogenic or xenogenic tissues and are popular for applications involving heart valves, blood vessels, tendons and ligaments. Importantly, this technique most closely mirrors the mechanical and biological properties of human tissue [33]. Complications from using this approach may arise if all cellular components of the donor tissue are not thoroughly removed prior to implantation, increasing the likelihood of immunological rejection, thereby requiring the long-term use of immunosuppressant drugs. Cell encapsulation in natural or synthetic hydrogel matrix is yet another method used in scaffold engineering, since these frameworks can be designed to provide biomimetic environments that polymerize from a liquid to a solid polymer network under specific conditions. By using a one-step procedure to encapsulate stem cells instead of topical cell seeding, a more homogenous cell density with exceptional cell viability is achieved. Here, we provide an overview of the field by examining a collection of synthetic scaffolds currently used in conjunction with ASCs to treat defects of various tissue types.

ASCs in synthetic scaffolds for cartilaginous regeneration

Cartilage is flexible connective tissue located in joints between bones, but regions of cartilaginous tissue also exist in the ear, nose and rib cage. Unlike bone, cartilage is not rigid; however, it is less flexible than muscle or other types of connective tissues, such as fat.

Cartilage is important in providing flexibility to the skeletal system, a critical feature that allows for proper function. Cartilage is primarily composed of chondrocytes, cells responsible for producing the ECM proteins required for the tissue's unique mechanical characteristics [34–37]. Cartilage is unable to self-repair after blunt-force trauma, athletic injury, disease or age-related degeneration. The number of knee surgeries to repair articular cartilage damage each year in the USA increases by 5% annually [38]. The natural lack of vascularization in addition to the minimal cell-to-cell contact restricts cartilage to only minimal spontaneous healing because of the slow dissemination of healing factors to distant cells. Because of these characteristics, treatments frequently consist of surgically removing damaged tissue in order to reduce pain and restore function [35,37,39]. A regenerative approach to cartilage replacement therapy involves the restoration of proper cellular morphology, and the prevention of further deterioration. Current treatments, such as allografting, can carry small, but serious risks of infection and disease transmission while treatments such as autologous chondrocytic transplantations may result in degenerative changes accompanied by pain [36,37,40].

ASCs can be induced into chondrogenic differentiation *in vitro* by the combinatorial influence of growth factors, such as TGF-β1 and TGF-β3, BMP-4 and bFGF. ASCs provide several advantages over autologous chondrocyte treatments because they do not induce an inflammatory response, form new cartilage and possess the potential for restoring long-term cartilage function. The use of 3D scaffolds has gained momentum in the field of cartilage restoration because of their ability to overcome the growth inhibition typically observed in standard *in vitro* cultures [41,42]. Synthetic platforms provide locations for ASCs to adhere, thereby providing an environment conducive for growth and proliferation. Additionally, scaffolds have also been shown to promote differentiation and enable cells to achieve a cartilage-like morphology and express chondro-specific molecules, such as COL2A1 and CSPCP [43].

Poly-lactide-co-glycolide (PLGA) is a copolymer approved for numerous therapeutic uses in humans by the US FDA since 2001. This copolymer may act as a stable or a biodegradable material depending on its formulation, and it possesses a permeable pore network that supports cell adhesion and proliferation. Mehlhorn and Zwingmann showed that these scaffolds were suitable cell carriers for chondrocytes. Furthermore, PLGA networks seeded with ASC-chondrocytes showed excellent volume stability and sufficient elasticity comparable to natural cartilage [44]. These results suggest that PLGA may serve as an effective scaffolding system for chondrocytes derived from ASCs.

Another avenue employs the use of fibrous polyglycolic acid (PGA) stabilized by polylactic acid (PLA). Cui *et al.* demonstrated that this combination of polymers produced promising results during the initial attachment of ASCs, and subsequent proliferation of chondrogenic-induced ASCs. In addition, cells deposited cartilage-specific ECM proteins within the polymer. Degradation times of approximately 2 months *in vivo* appeared to match the natural mechanisms of new cartilage formation. Thus, PGA/PLA in combination with ASCs may also serve as a synthetic scaffold for cartilage regeneration [43].

While PLGA and PGA/PLA comprise the bulk of synthetic polymers used for cartilage regeneration, other synthetic gels incorporate hyaluronic acid (HA), an important component of cartilage, into poly(ethylene)glycol (PEG) polymers. Unterman *et al.* showed that HA-interacting PEG hydrogels improved cartilage tissue formation *in vitro* and *in vivo* in instances where HA was presented at a later stage of differentiation, subsequently resulting in increased chondrogenic phenotypes [45]. Here, carefully considering properties of the native environment resulted in increased success by incorporating HA components that mimic the desired tissue. This is an important case that demonstrated functionalization of a scaffold to more closely replicate a desired environment had a positive effect on graft viability [46].

3D cell printing, or bioprinting, has become an increasingly attractive option for the treatment of bone lesions as it provides a means to create scaffold structures that alleviate the limitations of the fields due to the complex 3D geometries associated with defects. The use of cells in prepolymer 'bioink' allows a layer-by-layer deposition in a 3D construct that is analogous to tissues and organs [47,48]. This technique provides unique opportunities to develop complexly shaped scaffolds from synthetic material that encapsulate cells as shown by Lee *et al.* [49]. The fabrication of a structure with an ear shape with chondrocytes and adipocytes derived from ASC-derived cells in a polycaprolactone (PCL) hydrogel demonstrated a successful composite tissue. The efficient chondrogenesis and adipogenesis of the cell-printed structure resulted in a step forward for the practicality of 3D printing complex organs for tissue regeneration.

ASCs in synthetic scaffolds for osteogenic therapeutics

In contrast to cartilage, bone has regenerative capacity due to its inherent population of osteoblasts and osteoclasts (bone-forming and bone-resorbing cell types, respectively) [50]. However, these processes are frequently perturbed in cases of trauma, disease or

tumor resection. Bone autografts, in other words, harvesting bone from one anatomic site and grafting into another site in the same subject, is one of the primary approaches currently used for bone augmentation in a variety of orthopedic and maxillofacial procedures. Approximately 800,000 patients receive these grafts annually [51], and while significant skeletal incorporation has been observed in these types of grafts many drawbacks still exist using this approach, such as delayed healing, a complete failure to heal, morbidity at donor sites, quantity restrictions, substantial financial costs due to additional procedures to harvest transplant tissue and discomfort for the patient [52–55].

Collectively, focus has begun to shift toward the development of synthetic systems for use in conjunction with ASCs to replace traditional bone grafts. One study determined that PLGA is a viable scaffold for osteogenic differentiation of ASCs. After 2 weeks of osteogenic induction, mineralized nodular structures were observed by Alzarian Red and von Kossa staining, indicating successful calcification of the ECM [56]. The use of PLGA scaffolds for osteogenic differentiation provides a viable polymer scaffolding option, however, further investigation is needed to determine what external cues may be necessary prior to graft implantation of this particular material, which has shown promise for applications involving chondrogenic and adipogenic lineages; indicating that the basic polymer supports numerous cell fates and must be modified to help direct differentiation.

While polymers have proven to be useful in a variety of other fields, osteogenesis may require unique materials due to the highly specialized mechanical properties of natural bone. Thus, regenerative osteogenic technology has begun to employ the use of titanium metal to create a space that facilitates the migration of implanted cells and their osteogenic differentiation. Titanium is an inert biomaterial that possesses exceptional mechanical strength, is biocompatible and therefore, a prime candidate for use in regenerative applications involving bone. ASCs have shown compatibility with titanium systems, as well as displayed suitable cell adhesion. As a scaffold, titanium enables adhesion and osteoblastic differentiation of ASCs *in vitro*, indicated by an increased deposition of ALP and BGLAP (ECM proteins necessary for matrix mineralization) as well as calcification, confirmed by von Kossa staining [57,58]. The ability of ASCs to acquire the proper phenotypic differentiation as well as produce an ECM and a mineralized matrix suggest titanium as an attractive material as a filler or support structure for bone in growth in regenerative medicine [57].

Calcium phosphate ceramics (CPCs) are another class of scaffolds used for bone regeneration. These are promising synthetic materials due to their resemblance to bone mineral, their malleable bioactive properties and their surface characteristics, which support osteoblast adhesion, proliferation and differentiation *in vivo* [59,60]. Most CPCs examined have been shown to be osteoconductive (growth of bone on a surface) while only certain types exhibit osteoinductive (recruitment and differentiation of immature osteocytes) abilities. There is evidence, however, that increased mircoporosity increases the amount of bone inducing proteins secreted by ASCs *in vitro* [61]. The similarities of CPCs to bone, along with their ability to induce bone growth and promote secretion of important proteins elevate these materials as an intriguing and exciting possibility for osteogenic therapies.

While the similarities of CPC to bone have proven to be beneficial to osteogenic regeneration, the use of decellularized bone (DCB) in combination with PCL shows even greater promise. PCL is a biodegradable polyester polymer used to circumvent the inability of 3D printers to use DCB alone as a printing material. The use of 3D printers to engineer scaffolding systems using PCL has shown enhanced adhesion of ASCs. These cells exhibited significant upregulation of osteogenic genes such as *BGLAP*, *runx2* and *SPARC*. It was also demonstrated by Alzarian Red staining that ASCs on DCB:PCL materials showed increased calcification. When scaffolds were implanted into calvarial defects in mice, DCB:PCL scaffolds invoked nearly twice the volume of regenerated bone in 12 weeks compared with PCL alone [62].

The use of 3D-printed PCL scaffolding without addition of natural components has also shown by varying the internal pore size of the scaffold, it is possible to influence cell seeding of ASCs. By manipulating this parameter, Temple *et al.* were able to achieve optimal vascular and osteogenic differentiation in 3D-printed scaffolds [63]. This study also showed that maintenance of complex geometrical features such as maxilla and mandible bones maintains this porosity and therefore allows for cell seeding and vascularization similar to previous *in vivo* studies

Similar to PCL, polymers used in other regenerative studies, such PLGA can be blended with natural components to make them more amenable to 3D printing. Lee *et al.* determined that by 3D printing PLGA scaffolds impregnated with BMP-2 and ASCs, it is possible to achieve mandibular regeneration [64]. The use of a small-animal model of mandibular defects allows investigation of the potential for union of transplanted scaffolding with natural bone, within a site of segmental defect. Similarly, Kao *et al.* demonstrated that coating of 3D-printed PLA with bioinspired synthetic coatings increased the adhesion, proliferation, as well as the osteogenic and endothelial differentiation of ASCs in 3D structures [65]. These simple modifications to syn-

thetic 3D-printed scaffolds may serve as the basis for effective delivery carriers in bone tissue engineering.

ASCs in synthetic scaffolds for soft tissue regeneration

Soft-tissue defects are relatively common, accounting for nearly 10% of all emergency department visits in addition to causes previously examined (i.e., trauma, tumor resection) [66]. More than 100,000 breast reconstructions after mastectomy, and over 200,000 maxillofacial surgeries were performed in 2015 alone and it is predicted that there will be more than 12,000 new cases of soft-tissue sarcomas in the USA in 2016 [9,67]. The current treatment for many of these conditions is autologous lipotransfer, a procedure involving collecting fat tissue from a patient, minimally manipulating the resultant lipoaspirate and relocating it to the site of reconstruction [68–71]. Although used widely, reports show that there is extensive variability of long-term lipotransfer graft survival, due to unpredictable degrees of resorption and tissue volume loss that can range from 20 to 90% [32,72,73].

Variations in soft-tissue graft survival have been attributed to many causes including a lack of local angiogenesis, sample preparation, as well as innate properties of the transplant site [70]. In a national consensus survey, 92% of physicians stated that their patients experienced some degree of resorption, 52% reported a resorption rate of 50% or greater [74]. Mature adipocytes constitute the majority of the transplant volume, and since these cells are in a terminally differentiated state, they lack the ability for self-renewal and proliferation. The primary cause for transplant death is the lack of revascularization of the transplanted tissue. Success rates are often reported to be as low as 20%, while successful transplants are commonly attributed to the relatively small population of ASCs present in the transplanted fat, and can be enhanced by increasing the number of stem cells transplanted [70,75]. Thus, significant volume loss in these types of transplants provides motivation for finding ways to decrease the loss and thereby increase the likelihood of a successful transplant. The recent development of cell-assisted lipotransfer using concentrated ASCs as a lipoaspirate additive before transplantation leads to significantly improved results, specifically in terms of thickness gains observed during the first 6 months, and a reduction in thickness loss at 1 year [76]. However, even cases using stem cell enrichment, marginal volume losses were still documented, and in most cases no gain of regenerated tissue was reported [70]. Therefore, engineering synthetic scaffolds that can support the survival of the transplanted stem cell population while simultaneously promoting adipogenic differentiation has been proposed as a novel avenue for improving the success of these types of transplants.

Various synthetic scaffolding materials have been examined to determine structural viability for stem cell survival and adipose tissue reconstruction. Patrick *et al.* demonstrated that ASCs seeded into a PLGA scaffold and implanted subcutaneously into rats showed maximum adipose tissue formation after 2 months, but noted that between 3 and 12 months, a complete loss of reconstructed adipose tissue and degeneration of the PLGA scaffold occurred [77]. This loss of tissue may arise from the degradation of the scaffolding, especially since signs of PLGA degradation were apparent as early as 1 month post-transplantation. Thus, successful scaffolds for adipose tissue transplantation may require prolonged degradation times in order to allow for the maturation of regenerating tissue.

Cho *et al.* demonstrated that implanting a support made of PGA and PLA before injecting pre-adipocytes provided enough support to maintain the volume of the implants and showed regeneration of the adipose tissue after 6 weeks in athymic mice [78]. However, this approach utilizes an implant primarily acting as structural support for ASCs that are injected in a solution. Although stability of the transplanted volume was reported, there was no systematic method to measure pre-implantation volume, leading to difficulties in determining whether adipose growth was due to the implanted cells. Additionally, no conclusive evidence was shown to indicate that the regenerated cells originated from transplanted ASCs. In clinical applications, it will be imperative to determine that the incorporation and differentiation of implanted cells replaces missing tissue.

The use of blended copolymers has recently become increasingly popular for applications in therapeutic treatments. The blending of poly(glycerol sebacate) (PGS), a biodegradable and biocompatible synthetic elastomer specifically designed to imitate the mechanical behavior of soft tissue, with PLA (to overcome the quality and flexibility concerns of using PGS alone) has shown promise. Frydrych *et al.* showed that ASCs seeded onto the surface of a PGS/PLA scaffold exhibited significant amounts of cellular penetration and substantial collagen accumulation over 21 days [79]. However, *in vitro* degradation assays determined that degradation appeared to progress too rapidly (50% loss after ~30 days) for this scaffold to support the growth of target tissue, a phenomenon also observed by Patrick *et al.* [77].

Blending different scaffolding polymers provides the advantage of utilizing the positive attributes of each material. Lin *et al.* used mixtures of gelatin sponges and polyglycolic meshes encased in microfilament polypropylene mesh to support adipose tissue regeneration using predifferentiated ASCs [80]. The

Table 1. Synthetic scaffolds used in conjunction with adipose-derived stem cells

Scaffold material	Cartilage	Bone	Adipose
PLGA	Mehlhorn *et al.* (2009) [44]	Lee *et al.* (2008) [56] Lee *et al.* (2015) [64]	Patrick *et al.* (2002) [77]
PGA/PLA	Cui *et al.* (2009) [43]	–	Cho *et al.* (2005) [78]
HA-PEG	Unterman *et al.* (2012) [45]	–	–
PCL	Lee *et al.* (2014) [49]	Temple *et al.* (2014) [63]	–
Titanium	–	Gastaldi *et al.* (2010) [57] Marycz *et al.* (2015) [58]	–
CPC	–	Samavedi *et al.* (2013) [59] Barrere *et al.* (2006) [60] Li *et al.* (2011) [61]	–
DCB/PCL	–	Hung *et al.* (2016) [62]	–
PLA	–	Kao *et al.* (2015) [65]	–
PGS/PLA	–	–	Frydrych *et al.* (2015) [79]
Gelatin/PGA/PP	–	–	Lin *et al.* (2008) [80]
PEG	–	–	Clevenger *et al.* (2016) [88]

CPC: Calcium phosphate ceramic; DCB: Decellularized bone; HA: Hyaluronic acid; PCL: Polycaprolactone; PEG: Poly(ethylene)glycol; PGA: Polyglycolic acid; PGS: Poly(glycerol sebacate); PLA: Polylactic acid; PLGA: Poly-lactide-co-glycolide; PP: Polypropylene.

gelatin–polyglycolic mesh was observed to degrade completely within 60 days; however, the polypropylene mesh is biostable and remains as a permanent resident of the transplant procedure. In fact, it was demonstrated that after 6 months *in vivo* these scaffolds retained their shape, a trait attributed to the nondegradable mesh, while the newly formed adipose tissue occupied the space within the scaffold [80]. This avenue is an improvement in terms of the longevity of engineered adipose tissue; however, this system is complex and requires lengthy *in vitro* cultures, thus it may prove too difficult to translate to clinical applications.

While each of these synthetic scaffolds possesses positive attributes, each neglects to consider important interactions of cells with their surroundings. Immediately following seeding into a synthetic scaffold, cells must be afforded sites of adhesion from which they are able to receive signals for survival, proliferation and differentiation. Since these polymers are biologically inert, it is critical to engineer attachment sites that provide favorable interactions between the ASCs and their surroundings. PEG is a polymer that was approved for use in humans by the FDA in 1979, and is currently used in a myriad of applications ranging from food additives to pharmaceutical products and drug delivery systems [81,82]. Recently, it was demonstrated that incorporation of Arg-Gly-Asp (RGD) variant peptides (linear RGD, cyclic RGD and vitronectin-derived RGD) into PEG-based gels is a feasible approach to functionalizing an inert biomaterial [83–87]. These peptides provide sites for ASC attachment at the time of cell incorporation. It was demonstrated that various adhesion peptides provided transplanted ASCs with enhanced directed adipogenic differentiation by comparison to systems that contained no attachment peptide. Peptides considered to be highly adhesive lead to smaller lipid vacuoles and thus immature adipocytes. However, peptides containing RGD derived from vitronectin (less adhesive) allowed ASCs to attach when incorporated into the hydrogel, while remaining rounded morphologically [88]. This approach demonstrates that the initial environment encountered by ASCs may influence their ability to differentiate in 3D scaffolds.

Conclusion

Despite its relative youth, the field of regenerative medicine is expanding quickly, encompassing exciting developments in the area of bioengineering, stem cell biology and materials research. ASCs hold enormous potential in this field. The multipotency of ASCs provides the potential building blocks for the treatment and regeneration of damaged tissue. Their relative abundance, and their ease of access, suggests that ASCs may provide an improvement over other stem cells used in therapeutic treatments.

The design of complex and smart materials able to interact with cells to direct their biological response and differentiation has been on the rise since the advent of tissue engineering. It has been shown that the interactions of cells with their environment plays a critical role in their health and development [89]. In order to regenerate and restore healthy tissue after an insult, disease or defect the ability to direct implanted cells along specific pathways may prove to be paramount. There are

many avenues currently under investigation to determine the best method of combining ASCs and synthetic scaffolds to obtain an optimal graft or implant for the desired application. Table 1 summarizes various synthetic matrices that have been evaluated in the last 15 years for treatment of cartilage, bone and adipose tissue defects. One of the most common polymers, PLGA, has been used for all three purposes, showing positive results when used in osteogenic applications, neutral results when used in chongrogenic repair and a notable loss of volume when applied to cases of adipogenic tissue growth. This is a prime example of the diverse capability of synthetic polymers used with stem cell populations. It is critical to consider the downstream consequences for all proposed scaffolding materials; specifically, scaffolding systems successfully used in one tissue type may not be yield similar results in another. Mimicking the native environment of the target tissue is likely to play a significant role for the long-term survival of virtually all transplant scaffolds.

Indeed, it was recently demonstrated that various adhesion peptides provided transplanted ASCs with enhanced directed adipogenic differentiation by comparison to systems that contained no attachment peptide [88]. The use of vitronectin-derived attachment peptides promoted the development of larger lipid vacuoles, further suggesting that the interaction of the ASCs with their scaffolding may have a significance impact on the desired differentiation and health of implanted cells [90,91]. Biomimetic PEG hydrogels may prove to be superior synthetic scaffolds for use in tissue reconstruction [92–94].

Future perspective

Applications of adipose-derived stem cell therapies have enormous potential for expanding the field of regenerative medicine. Their ability to differentiate into numerous cell types, as well as their abundance, places ASCs at the forefront in the development of next-generation therapeutic treatments. Vascularization of grafts and implants is another chief concern with respect to cell viability. This is a critical issue in current approaches for regeneration and treatment, and thus an important factor to address when developing new synthetic scaffold systems. The ability of ASCs to differentiate into endothelial cells along with a scaffold that supports a desired differentiation may increase the chances of achieving a scaffold that produces viable, long-lasting, vascularized tissue [95–98].

Transitioning scaffolding materials from the laboratory to clinical applications poses challenges that require further investigation. For example, additional demonstration of long-term safety in preclinical animal models will be necessary prior to their use in clinical applications. This process is timely, labor-intensive and expensive; however, the treatment benefits will outweigh the initial hurdles encountered in the exploration and development of synthetic scaffold for use as regenerative therapeutics.

Disclaimer

The content within does not necessarily reflect the position or policy of the government, and endorsement should not be inferred.

Financial & competing interests disclosure

This work was supported by the California Institute for Regenerative Medicine (CIRM; DR1-01444, CL1-00521, TB1-01177, TG2-01151 and FA1-00616) to DO Clegg, the National Science Foundation (IIS-0808772 and ITR-0331697) to SK Fisher and a grant to the University of California Santa Barbara Institute for Collaborative Biotechnologies from the US Army Research Office (W911NF-09-0001) to DO Clegg. TN Clevenger was a predoctoral fellow of the California Institute for Regenerative Medicine. The authors have no other relevant affiliations or financial involvement with any organization or entity with a financial interest in or financial conflict with the subject matter or materials discussed in the manuscript apart from those disclosed.

No writing assistance was utilized in the production of this manuscript.

Executive summary

Adipose stem cells in synthetic scaffolds for cartilaginous regeneration

- Synthetic scaffolds made from polymers such as poly-lactide-co-glycolide (PLGA), polyglycolic acid/polylactic acid (PLA) and poly(ethylene)glycol show the ability for adipose-derived stem cells (ASCs) to survive and differentiate along a chondrogenic lineage.

ASCs in synthetic scaffolds for osteogenic therapies

- Titanium, calcium phosphate ceramics and PLGA promote the mineralization of extracellular matrix secreted by ASC-derived osteocytes.

ASCs in synthetic scaffolds for adipogenic replacement

- PLGA, polyglycolic acid/PLA and polyglycerol sebacate/PLA are all blends of synthetic polymers that have been used in the adipogenic differentiation of ASCs.
- Poly(ethylene)glycol scaffolds containing different adhesive peptides have shown the *in vivo* influence the adipogenic differentiation of ASCs.

References

Papers of special note have been highlighted as:
• of interest; •• of considerable interest

1 Atala A, Lanza RP. *Methods of Tissue Engineering.* Gulf Professional Publishing, San Diego, CA, USA (2002).

2 Mao AS, Mooney DJ. Regenerative medicine: current therapies and future directions. *Proc. Natl Acad. Sci. USA* 112(47), 14452–14459 (2015).

3 Mironov V, Visconti RP, Markwald RR. What is regenerative medicine? Emergence of applied stem cell and developmental biology. *Expert Opin. Biol. Ther.* 4(6), 773–781 (2004).

4 Kaiser LR. The future of multihospital systems. *Top Health Care Financ.* 18(4), 32–45 (1992).

5 Thomson JA. Embryonic stem cell lines derived from human blastocysts. *Science* 282(5391), 1145–1147 (1998).

6 Tibbitt MW, Rodell CB, Burdick JA, Anseth KS. Progress in material design for biomedical applications. *Proc. Natl Acad. Sci. USA* 112(47), 1444–14451 (2015).

7 Harrison RH, St-Pierre J-P, Stevens MM. Tissue engineering and regenerative medicine: a year in review. *Tissue Eng. Part B Rev.* 20(1), 1–16 (2014).

8 Marine D, Manley OT. Homeotransplantation and autotransplantation of the spleen in rabbits: III. Further data on growth, permanence, effect of age, and partial or complete removal of the spleen. *J. Exp. Med.* 32(1), 113–133 (1920).

9 Surgeons ASOP. 2015 Cosmetic Plastic Surgery Statistics. 1–3 (2016). www.plasticsurgery.org/Documents

10 Peng L, Xie D-Y, Lin B-L *et al.* Autologous bone marrow mesenchymal stem cell transplantation in liver failure patients caused by hepatitis B: short-term and long-term outcomes. *Hepatology* 54(3), 820–828 (2011).

11 De Francesco F, Ricci G, D'Andrea F, Nicoletti GF, Ferraro GA. Human adipose stem cells: from bench to bedside. *Tissue Eng. Part B Rev.* 21(6), 572–584 (2015).

12 Pittenger MF, Mackay AM, Beck SC *et al.* Multilineage potential of adult human mesenchymal stem cells. *Science* 284(5411), 143–147 (1999).

13 Sung HJ, Hong SC, Yoo JH *et al.* Stemness evaluation of mesenchymal stem cells from placentas according to developmental stage: comparison to those from adult bone marrow. *J. Korean Med. Sci.* 25(10), 1418 (2010).

14 Baer PC, Griesche N, Luttmann W, Schubert R, Luttmann A, Geiger H. Human adipose-derived mesenchymal stem cells *in vitro*: evaluation of an optimal expansion medium preserving stemness. *Cytotherapy* 12(1), 96–106 (2012).

15 Yu J, Tu Y-K, Tang Y-B, Cheng N-C. Stemness and transdifferentiation of adipose-derived stem cells using L-ascorbic acid 2-phosphate-induced cell sheet formation. *Biomaterials* 35(11), 3516–3526 (2014).

16 Bourin P, Bunnell BA, Casteilla L *et al.* Stromal cells from the adipose tissue-derived stromal vascular fraction and culture expanded adipose tissue-derived stromal/stem cells: a joint statement of the International Federation for Adipose Therapeutics and Science (IFATS) and the International Society for Cellular Therapy (ISCT). *Cytotherapy* 15(6), 641–648 (2013).

•• **Seminal publication on the definition of adipose stem cells.**

17 MD MD, Le Blanc K, Mueller I *et al.* Minimal criteria for defining multipotent mesenchymal stromal cells. The International Society for Cellular Therapy position statement. *Cytotherapy* 8(4), 315–317 (2012).

18 Zuk PA, Zhu M, Ashjian P *et al.* Human adipose tissue is a source of multipotent stem cells. *Mol. Biol. Cell* 13(12), 4279–4295 (2002).

19 Bernacki SH, Wall ME, Loboa EG. Isolation of human mesenchymal stem cells from bone and adipose tissue. In: *Methods in Cell Biology.* Elsevier, San Diego, CA, USA, 257–278 (2008).

20 Baer PC. Adipose-derived mesenchymal stromal/stem cells: an update on their phenotype *in vivo* and *in vitro*. *WJSC* 6(3), 256 (2014).

•• **Excellent review on the current state of the adipose stem cell field.**

21 Baer PC, Geiger H. Adipose-derived mesenchymal stromal/stem cells: tissue localization, characterization, and heterogeneity. *Stem Cells Int.* 2012(3), 1–11 (2012).

22 Fraser JK, Zhu M, Wulur I, Alfonso Z. Adipose-derived stem cells. *Methods Mol. Biol.* 449, 59–67 (2008).

23 Strioga M, Viswanathan S, Darinskas A, Slaby O, Michalek J. Same or not the same? Comparison of adipose tissue-derived versus bone marrow-derived mesenchymal stem and stromal cells. *Stem Cells Dev.* 21(14), 2724–2752 (2012).

24 Baer PC, Kuçi S, Krause M *et al.* Comprehensive phenotypic characterization of human adipose-derived stromal/stem cells and their subsets by a high throughput technology. *Stem Cells Dev.* 22(2), 330–339 (2013).

25 Noël D, Caton D, Roche S, Bony C, Lehmann S. Cell specific differences between human adipose-derived and mesenchymal-stromal cells despite similar differentiation potentials. *Exp. Cell Res.* 314(7), 1575–1584 (2008).

26 Zhu X, Shi W, Tai W, Liu F. The comparition of biological characteristics and multilineage differentiation of bone marrow and adipose derived mesenchymal stem cells. *Cell Tissue Res.* 350(2), 277–287 (2012).

27 Peng L, Jia Z, Yin X *et al.* Comparative analysis of mesenchymal stem cells from bone marrow, cartilage, and adipose tissue. *Stem Cells Dev.* 17(4), 761–774 (2008).

28 Wankhade UD, Shen M, Kolhe R, Fulzele S. Advances in adipose-derived stem cells isolation, characterization, and application in regenerative tissue engineering. *Stem Cells Int.* 2016(5), 1–9 (2016).

29 Lim M-H, Kim HW, Paik K-C, Cho SC, Yoon DY, Lee H-J. Association of the DAT1 polymorphism with attention deficit hyperactivity disorder (ADHD): a family-based approach. *Am. J. Med. Genet. B Neuropsychiatr. Genet.* 141B(3), 309–311 (2006).

30 Lim MH, Ong WK, Sugii S. The current landscape of adipose-derived stem cells in clinical applications. *Expert Rev. Mol. Med.* 16, e8 (2014).

31 Minteer DM, Marra KG, Rubin JP. Adipose stem cells. *Clin. Plast. Surg.* 42(2), 169–179 (2015).

32 Chan CW, McCulley SJ, Macmillan RD. Autologous fat transfer – a review of the literature with a focus on breast cancer surgery. *Br. J. Plast. Surg.* 61(12), 1438–1448 (2008).

33 Petit F, Minns AB, Dubernard J-M, Hettiaratchy S, Lee WPA. Composite tissue allotransplantation and reconstructive surgery: first clinical applications. *Ann. Surg.* 237(1), 19–25 (2003).

34 Behonick DJ, Werb Z. A bit of give and take: the relationship between the extracellular matrix and the developing chondrocyte. 120(11), 1327–1336 (2003).

35 Kölliker A. *Manual of Human Histology.* Syndenham Society, London, UK (1853).

36 Breinan HA, Minas T, Hsu HP, Nehrer S, Sledge CB, Spector M. Effect of cultured autologous chondrocytes on repair of chondral defects in a canine model. *J. Bone Joint Surg. Am.* 79(10), 1439–1451 (1997).

37 Mobasheri A, Csaki C, Clutterbuck AL, Rahmanzadeh M, Shakibaei M. Mesenchymal stem cells in connective tissue engineering and regenerative medicine: applications in cartilage repair and osteoarthritis therapy. *Histol. Histopathol.* 24(3), 347–366 (2009).

38 McCormick F, Harris JD, Abram GD *et al.* Trends in the surgical treatment of articular cartilage lesions in the United States: an analysis of a large private-payer database over a period of 8 years. *Arthroscopy* 30(2), 222–226 (2014).

39 Campbell CJ. The healing of cartilage defects. *Clin. Orthop. Relat. Res.* 64, 45–63 (1969).

40 Centers for Disease Control and Prevention (CDC). Update: allograft-associated bacterial infections – United States, 2002. *MMWR Morb. Mortal Wkly Rep.* 51(10), 207–210 (2002).

41 Xu J, Wang W, Ludeman M *et al.* Chondrogenic differentiation of human mesenchymal stem cells in three-dimensional alginate gels. *Tissue Eng. Part A* 14(5), 667–680 (2008).

42 Sun AX, Lin H, Beck AM, Kilroy EJ, Tuan RS. Projection stereolithographic fabrication of human adipose stem cell-incorporated biodegradable scaffolds for cartilage tissue engineering. *Front Bioeng. Biotechnol.* 3, 115 (2015).

43 Cui L, Wu Y, Cen L *et al.* Repair of articular cartilage defect in non-weight bearing areas using adipose derived stem cells loaded polyglycolic acid mesh. *Biomaterials* 30(14), 2683–2693 (2009).

44 Mehlhorn AT, Zwingmann J. Chondrogenesis of adipose-derived adult stem cells in a poly-lactide-co-glycolide scaffold. *Tissue Eng. Part A* 15(5), 1159–1167 (2009).

45 Unterman SA, Gibson M, Lee JH *et al.* Hyaluronic acid-binding scaffold for articular cartilage repair. *Tissue Eng. Part A* 18(23–24), 2497–2506 (2012).

46 DeForest CA, Anseth KS. Advances in bioactive hydrogels to probe and direct cell fate. *Annu. Rev. Chem. Biomol. Eng.* 3(1), 421–444 (2012).

47 Mandrycky C, Wang Z, Kim K, Kim D-H. 3D bioprinting for engineering complex tissues. *Biotechnol. Adv.* 34(4), 422–434 (2016).

48 Bajaj P, Schweller RM, Khademhosseini A, West JL, Bashir R. 3D biofabrication strategies for tissue engineering and regenerative medicine. *Annu. Rev. Biomed. Eng.* 16(1), 247–276 (2014).

49 Lee J-S, Hong JM, Jung JW, Shim J-H, Oh J-H, Cho D-W. 3D printing of composite tissue with complex shape applied to ear regeneration. *Biofabrication* 6(2), 024103 (2014).

50 Rodan GA, Martin TJ. Role of osteoblasts in hormonal control of bone resorption – a hypothesis. *Calcif. Tissue Int.* 33(4), 349–351 (1981).

51 Laurencin CT, Ambrosio AM, Borden MD, Cooper JA. Tissue engineering: orthopedic applications. *Annu. Rev. Biomed. Eng.* 1, 19–46 (1999).

52 Prolo DJ, Rodrigo JJ. Contemporary bone graft physiology and surgery. *Clin. Orthop. Relat. Res.* (200), 322–342 (1985).

53 Couture J, Cabana F. Irradiated allograft bone in spine surgery. *Spine* 38(7), 558–563 (2013).

54 Ahlmann E, Patzakis M, Roidis N, Shepherd L, Holtom P. Comparison of anterior and posterior iliac crest bone grafts in terms of harvest-site morbidity and functional outcomes. *J. Bone Joint Surg. Am.* 84-A(5), 716–720 (2002).

55 St John TA, Vaccaro AR, Sah AP *et al.* Physical and monetary costs associated with autogenous bone graft harvesting. *Am J. Orthop.* 32(1), 18–23 (2003).

56 Lee JH, Rhie J-W, Oh DY, Ahn ST. Osteogenic differentiation of human adipose tissue-derived stromal cells (hASCs) in a porous three-dimensional scaffold. *Biochem. Biophys. Res. Commun.* 370(3), 456–460 (2008).

57 Gastaldi G, Asti A, Scaffino MF *et al.* Human adipose-derived stem cells (hASCs) proliferate and differentiate in osteoblast-like cells on trabecular titanium scaffolds. *J. Biomed. Mater. Res. A* 94(3), 790–799 (2010).

58 Marycz K, Śmieszek A, Grzesiak J *et al.* The osteogenic properties of multipotent mesenchymal stromal cells in cultures on TiO_2 sol-gel-derived biomaterial. *BioMed. Res. Int.* 2015(1), 1–11 (2015).

59 Samavedi S, Whittington AR, Goldstein AS. Calcium phosphate ceramics in bone tissue engineering: a review of properties and their influence on cell behavior. *Acta Biomater.* 9(9), 8037–8045 (2013).

60 Barrère F, van Blitterswijk CA, de Groot K. Bone regeneration: molecular and cellular interactions with calcium phosphate ceramics. *Int. J. Nanomedicine* 1(3), 317–332 (2006).

61 Li X, Liu H, Niu X *et al.* Osteogenic differentiation of human adipose-derived stem cells induced by osteoinductive calcium phosphate ceramics. *J. Biomed. Mater. Res.* 97B(1), 10–19 (2011).

62 Hung BP, Naved BA, Nyberg EL *et al.* Three-dimensional printing of bone extracellular matrix for craniofacial regeneration. *ACS Biomater. Sci. Eng.* doi:10.1021/acsbiomaterials.6b00101 (2016) (Epub ahead of print).

•• **Innovative study combining 3D printing and stem cells for regenerative therapy.**

63 Temple JP, Hutton DL, Hung BP *et al.* Engineering anatomically shaped vascularized bone grafts with hASCs and 3D-printed PCL scaffolds. *J. Biomed. Mater. Res. A* 102(12), 4317–4325 (2014).

64 Lee MK, DeConde AS, Lee M *et al.* Biomimetic scaffolds facilitate healing of critical-sized segmental mandibular defects. *Am. J. Otolaryngol.* 36(1), 1–6 (2015).

65 Kao CT, Lin CC, Chen YW, Yeh CH, Fang HY, Shie MY. Poly(dopamine) coating of 3D printed poly(lactic acid) scaffolds for bone tissue engineering. *Mater. Sci. Eng. C Mater. Biol. Appl.* 56, 165–173 (2015).

66 Ong TK, Dudley M. Craniofacial trauma presenting at an adult accident and emergency department with an emphasis on soft tissue injuries. *Injury* 30(5), 357–363 (1999).

67 Cancer Society A. Cancer facts. 1–72 (2015). www.cancer.org/acs/groups/content

68 Kantanen DJ, Closmann JJ, Rowshan HH. Abdominal fat harvest technique and its uses in maxillofacial surgery. *Oral Surg. Oral Med. Oral Pathol. Oral Radiol. Endod.* 109(3), 367–371 (2010).

69 Yoshimura K, Asano Y, Aoi N *et al.* Progenitor-enriched adipose tissue transplantation as rescue for breast implant complications. *Breast J.* 16(2), 169–175 (2010).

• **Currently, the most efficient treatment of soft tissue defects.**

70 Domenis R, Lazzaro L, Calabrese S *et al.* Adipose tissue derived stem cells: *in vitro* and *in vivo* analysis of a standard and three commercially available cell-assisted lipotransfer techniques. *Stem Cell Res. Ther.* 6, 2 (2015).

71 Hammer-Hansen N, Akram J, Damsgaard TE. The versatility of autologous fat transplantation in correction of facial deformities: a single-center experience. *Plast. Surg. Int.* 2015, 703535 (2015).

72 Toyserkani NM, Quaade ML, Sørensen JA. Cell-assisted lipotransfer: a systematic review of its efficacy. *Aesth. Plast. Surg.* 40(2), 309–318 (2016).

73 Parrish JN, Metzinger SE. Autogenous fat grafting and breast augmentation: a review of the literature. *Aesthet. Surg. J.* 30(4), 549–556 (2010).

74 Kaufman MR, Bradley JP, Dickinson B *et al.* Autologous fat transfer national consensus survey: trends in techniques for harvest, preparation, and application, and perception of short- and long-term results. *Plast. Reconstr. Surg.* 119(1), 323–331 (2007).

75 Coleman SR. Facial augmentation with structural fat grafting. *Clin. Plast. Surg.* 33(4), 567–577 (2006).

76 Yoshimura K, Sato K, Aoi N, Kurita M, Hirohi T, Harii K. Cell-assisted lipotransfer for cosmetic breast augmentation: supportive use of adipose-derived stem/stromal cells. *Aesth. Plast. Surg.* 32(1), 48–55 (2007).

77 Patrick CW Jr, Zheng B, Johnston C. Long-term implantation of preadipocyte-seeded PLGA scaffolds. *Tissue Eng.* 8(2), 283–293 (2002).

78 Cho SW, Kim SS, Rhie JW, Cho HM, Choi CY, Kim BS. Engineering of volume-stable adipose tissues. *Biomaterials* 26(17), 3577–3585 (2005).

79 Frydrych M, Román S, MacNeil S, Chen B. Biomimetic poly(glycerol sebacate)/poly(l-lactic acid) blend scaffolds for adipose tissue engineering. *Acta Biomater.* 18, 40–49 (2015).

80 Lin S-D, Wang K-H, Kao A-P. Engineered adipose tissue of predefined shape and dimensions from human adipose-derived mesenchymal stem cells. *Tissue Eng. Part A* 14(5), 571–581 (2008).

81 FIP E. Opinion of the scientific panel on food additives, flavourings, processing aids and materials in contact with food on a request from the commission related to an application on the use of polyethylene glycol (PEG) as a film coating agent for use in food supplement products. 1–22 (2007). www.efsa.europa.eu/sites/default

82 Knop K, Hoogenboom R, Fischer D, Schubert US. Poly(ethylene glycol) in drug delivery: pros and cons as well as potential alternatives. *Angew. Chem. Int. Ed. Engl.* 49(36), 6288–6308 (2010).

83 Hwang NS, Varghese S, Lee HJ, Zhang Z, Elisseeff J. Biomaterials directed *in vivo* osteogenic differentiation of mesenchymal cells derived from human embryonic stem cells. *Tissue Eng. Part A* 19(15–16), 1723–1732 (2013).

84 Mann BK, Gobin AS, Tsai AT, Schmedlen RH, West JL. Smooth muscle cell growth in photopolymerized hydrogels with cell adhesive and proteolytically degradable domains: synthetic ECM analogs for tissue engineering. *Biomaterials* 22(22), 3045–3051 (2001).

85 Peyton SR, Raub CB, Keschrumrus VP, Putnam AJ. The use of poly(ethylene glycol) hydrogels to investigate the impact of ECM chemistry and mechanics on smooth muscle cells. *Biomaterials* 27(28), 4881–4893 (2006).

86 Lutolf MP, Hubbell JA. Synthetic biomaterials as instructive extracellular microenvironments for morphogenesis in tissue engineering. *Nat. Biotechnol.* 23(1), 47–55 (2005).

87 Hersel U, Dahmen C, Kessler H. RGD modified polymers: biomaterials for stimulated cell adhesion and beyond. *Biomaterials* 24(24), 4385–4415 (2003).

88 Clevenger TN, Hinman CR, Ashley Rubin RK *et al.* Vitronectin-based, biomimetic encapsulating hydrogel scaffolds support adipogenesis of adipose stem cells. *Tissue Eng. Part A* 22(7–8), 597–609 (2016).

89 Engler AJ, Sen S, Sweeney HL, Discher DE. Matrix elasticity directs stem cell lineage specification. *Cell* 126(4), 677–689 (2006).

•• **Critical paper on the effects the matrix has on stem cell differentiation.**

90 Cukierman E, Pankov R, Stevens DR, Yamada KM. Taking cell-matrix adhesions to the third dimension. *Science* 294(5547), 1708–1712 (2001).

91 Konttinen YT, Kaivosoja E, Stegaev V *et al. Extracellular Matrix and Tissue Regeneration.* Springer, Dordrecht, The Netherlands, 21–80 (2010).

92 Amer LD, Holtzinger A, Keller G, Mahoney MJ, Bryant SJ. Enzymatically degradable poly(ethylene glycol) hydrogels for the 3D culture and release of human embryonic stem cell derived pancreatic precursor cell aggregates. *Acta Biomater.* 22, 103–110 (2015).

93 Sridhar BV, Brock JL, Silver JS, Leight JL, Randolph MA, Anseth KS. Development of a cellularly degradable PEG hydrogel to promote articular cartilage extracellular matrix deposition. *Adv. Healthc. Mater.* 4(5), 702–713 (2015).

94 Stevens KR, Miller JS, Blakely BL, Chen CS, Bhatia SN. Degradable hydrogels derived from PEG-diacrylamide for hepatic tissue engineering. *J. Biomed. Mater. Res. A* 103(10), 3331–3338 (2015).

95 Szöke K, Beckstrøm KJ, Brinchmann JE. Human adipose tissue as a source of cells with angiogenic potential. *Cell Transplant.* 21(1), 235–250 (2012).

96 Cao Y, Sun Z, Liao L, Meng Y, Han Q, Zhao RC. Human adipose tissue-derived stem cells differentiate into endothelial cells *in vitro* and improve postnatal neovascularization *in vivo*. *Biochem. Biophys. Res. Commun.* 332(2), 370–379 (2005).

97 Rehman J. Secretion of angiogenic and antiapoptotic factors by human adipose stromal cells. *Circulation* 109(10), 1292–1298 (2004).

98 Zanotelli MR, Ardalani H, Zhang J *et al.* Stable engineered vascular networks from human induced pluripotent stem cell-derived endothelial cells cultured in synthetic hydrogels. *Acta Biomater.* 35, 32–41 (2016).